



Investigation of Tribological Behavior of Plasma Sprayed NiTi Coating for Aerospace Application

B. Swain¹ · S. Mantry² · S. S. Mohapatra³ · S. C. Mishra¹ · A. Behera¹

Submitted: 24 December 2021 / in revised form: 2 August 2022 / Accepted: 2 August 2022 / Published online: 18 August 2022
© ASM International 2022

Abstract In the absence of any literature regarding the development of erosion resistance protective coatings on the aerospace engine parts using NiTi alloy, the current work has been focused on the detail investigation of the solid particle erosion resistance of the NiTi coating developed by atmospheric plasma spray technique. The coating has been prepared by considering an elemental mixture of equiatomic Ni and Ti powder as feedstock material with different plasma arc currents and primary gas flow rates. The quality of the coatings has been checked by different characterization techniques like x-ray diffraction, scanning electron microscopy and energy-dispersive spectroscopy. The defects observed from the microstructural investigation sometimes lead to more erosion and sometimes resulted in less erosion rate. The investigation of the effect of the porosity percentage on the erosion rate revealed that as the porosity percentage increases, the erosion rate increases at both 45° and 90° erodent impingement angles due to the lack in strength at the edges of the pores. Furthermore, the surface area of the roughness peaks, the stress concentration at the gap between the roughness peaks and height of the surface profile are mainly responsible for the erosion performance at both the erodent impact angles. The erosion rate is inversely

proportional to the microhardness of the coatings. In addition to the above, according to the results disclosed by the erosion performance at different impingement angles, the coating is brittle in nature. The surface morphological study of the eroded coatings indicated various erosion mechanisms like plastic deformation, plowing, microcutting, lip formation, scratches, groove formation on the coatings impinged at 45° impact angle and groove formation, splat fracture, splat fragmentation, splat delamination, pit formation on the coatings impinged at 90° impingement angle.

Keywords coating · NITINOL · plasma spray · solid particle erosion · surface morphology

Introduction

In the current world, various material degradation phenomena have been noticed in the aerospace industries. Among all of them, solid particle erosion (SPE) wear is a type of material degradation phenomenon where the surface is damaged by the interaction of the erodent with its momentum and kinetic energy. Various components like helicopter rotor blades (Ref 1), compressor and turbine blades (Ref 2-5) of gas turbine engine, wind shields (Ref 6) or any exposed area of an aircraft experienced the detrimental effects of solid particle erosion. The research on the solid particle erosion has been carried out for more than 50 yrs. However, the surface protection from the solid particle erosion wear has been started in late 80 s by USSR for the protection of aircrafts in the extreme environments of Afghanistan. Thereafter, in 1990s, at the time of first Gulf war, Royal air force of the Great Britain reported a life span of 20 h of a helicopter engine due to the effect of solid particle erosion surface degradation phenomenon (Ref 7). After that, the SPE

✉ B. Swain
enggbiswajit92@gmail.com

¹ Advanced Materials Processing and Research Laboratory (AMPRE-Lab), Department of Metallurgical and Materials Engineering, National Institute of Technology, Rourkela, Odisha 769008, India

² Material Chemistry Department, CSIR-Institute of Minerals and Materials Technology, Bhubaneswar, Odisha 751013, India

³ Department of Chemical Engineering, National Institute of Technology, Rourkela, Odisha 769008, India

grabbed the attention of the researchers. In the follow-up research, in 2004, Pratt and Whitney declared the modification of F135 engine of F35 joint strike fighter due to the effect of SPE (Ref 8). To avoid the effects of SPE, various attempts have been made. However, surface coating technology has been proved as the most effective process to restrict the effect of SPE. According to the researchers, the material selection for the development of the coating plays a vital role for any application.

In the path of the selection of the coating material, the NiTi alloy has been noticed due to its two excellent magic properties such as pseudoelasticity and shape memory effect (Ref 9, 10). However, except these two properties, the NiTi has many other excellent properties like corrosion and wear resistance (Ref 11–13), water erosion resistance (Ref 14), hardness at high temperature (Ref 15), high damping behavior (Ref 16), high strength at fatigue load (Ref 17), etc. The abovementioned properties extend the range of application of the NiTi alloy. However, due to these excellent properties, the cost of the NiTi is very high, and thus, the use of bulk NiTi material is not economical. Therefore, to achieve these properties of NiTi in an economical way, the coating of this material has been developed.

Among all the coating technologies, the thermal spray coating has been proved as the most significant process. Among all the thermal spray processes, plasma spray coating process has been mostly chosen for the industrial applications (Ref 18–21) due to its excellent properties like wear resistance, corrosion resistance, cavitation erosion resistance, high temperature stability, mechanical and electrical properties, etc., which are the required properties in the harsh environments. In the plasma spray coating process, the powder from the feedstock flows to the plasma gun by carrier gas and experiences through the plasma plume (Ref 22–25). Then, the molten or semi-molten particles are deposited on the substrate or pre-deposited splats (Ref 26–33). The plasma spray coating processes are of two types, i.e., vacuum plasma spraying (VPS) and atmospheric plasma spraying (APS). The VPS is much costly process as compared to APS and not suitable for low cost applications. Furthermore, it cannot be used in many industrial applications due to its inability to coat intricate parts. In addition to the above, the energy consumption is more in the detonation gun spray. In flame spray technology, the nature of feed stock is metal alloys, polymers and cermets, in wire arc spraying, the nature of feed stock is mostly conductive wires, in HVOF, HVOF and D-gun technologies, the feed stock is mostly metal and cermets. However, in plasma spray technology, the all type of materials can be considered as feed stock. Therefore, in the current investigation, the APS process has been considered as coating methodology.

Various literature works have been reported on the thermal spray coating of NiTi alloy. Cinca et al. (Ref 34)

developed NiTi coating by three different thermal spray processes, i.e., VPS, HVOF and APS. They have also investigated the wear property of the coating by ball-on-disk wear test and concluded that the coating developed by APS method has the best wear resistance among all the three processes. Hiraga et al. (Ref 35) prepared NiTi coating by laser plasma hybrid spraying process and investigated the cavitation erosion performance of the coating. They noticed that the NiTi coating has an excellent cavitation erosion resistance which is approximately 380-fold of the Ti-6Al-4 V. In the follow-up research, Guilemany et al. (Ref 36) revealed the corrosion resistance property of the NiTi coatings developed by APS, VPS and HVOF processes. Shi et al. (Ref 37) investigated the cavitation erosion and jet impingement erosion properties of APS NiTi coating. However, no literature works have been found regarding the solid particle erosion performance of the NiTi coating except some of the works reported in our previous articles (Ref 38–41). Swain et al. (Ref 38) investigated the mechanical properties and solid particle erosion wear phenomenon of the coatings developed at four different plasma arc currents. Swain et al. (Ref 39) analyzed the microstructure and solid particle erosion of the coating developed at a single parameter. Furthermore, the mechanical properties and erosion property of the coatings developed at different stand-off distances have been investigated in Swain et al. (Ref 40). In the follow-up research, in Swain et al. (Ref 41), a few discussion on the erosion property of the coating developed at optimized process parameters has been performed. However, in all our previous articles, the effect of various coating physical and mechanical properties like microstructure, phase and composition, porosity, surface roughness, microhardness and erosion impact parameters like erosion impingement angle on the SPE phenomenon of the plasma sprayed NiTi coating is still unrevealed. Therefore, in the current investigation, a correlation between coating properties and SPE has been established. In addition to the above, the surface morphologies of the coatings impinged at different erodent impingement angles have also been analyzed.

Materials and Methods

Materials

An elemental mixture of equiatomic Ni (99.9% purity) and Ti (99.9% purity) has been taken as feedstock material. The mean particle diameters of Ni and Ti powders are 35.27 and 33.93 μm , respectively. For the economic perspective, mild steel (AISI-1018) of dimension (50 × 40 × 5 mm) has been considered as the substrate material.

Methods

Atmospheric Plasma Spray Coating

An atmospheric plasma spraying equipment of nozzle diameter 6 mm has been used for the coating purpose. Before the coating process, the substrate has been sand blasted by Al_2O_3 grits to enhance the mechanical interlocking and adhesion property of the coating. Furthermore, the substrate was preheated before coating process for better heat transfer between coating and the substrate material. The Ar gas has been used as both primary and carrier gas, and H_2 was used as the secondary

gas. The coating has been developed by the to and fro motion of the nozzle with the help of a six-axis robot. After coating process, a cooling operation has been performed with a cooling rate of 10^6 K/s. The plasms spray process parameters are listed in Table 1.

Solid Particle Erosion Wear Test

The solid particle erosion test has been performed according to the ASTM G76 method (Ref 45) using air jet erosion test rig (Model: Magnum Engineers, India) (Fig. 1). The test rig includes an air compressor, particle

Table 1 Plasma spray coating parameters

APS parameters	Values	Justification
Substrate temperature ($^{\circ}\text{C}$)	120	According to the literature (Ref 36, 42-44)
Powder feed rate (g/min)	60	
Primary gas (Ar) flow rate (L/min)	35, 40, 45	
Carrier gas (Ar) flow rate (L/min)	3.5	
Secondary gas (H_2) flow rate (L/min)	8	
Stand-off distance (mm)	120	
Number of cycles	7	
Current (A)	400, 450, 500, 550	
Voltage (V)	70	

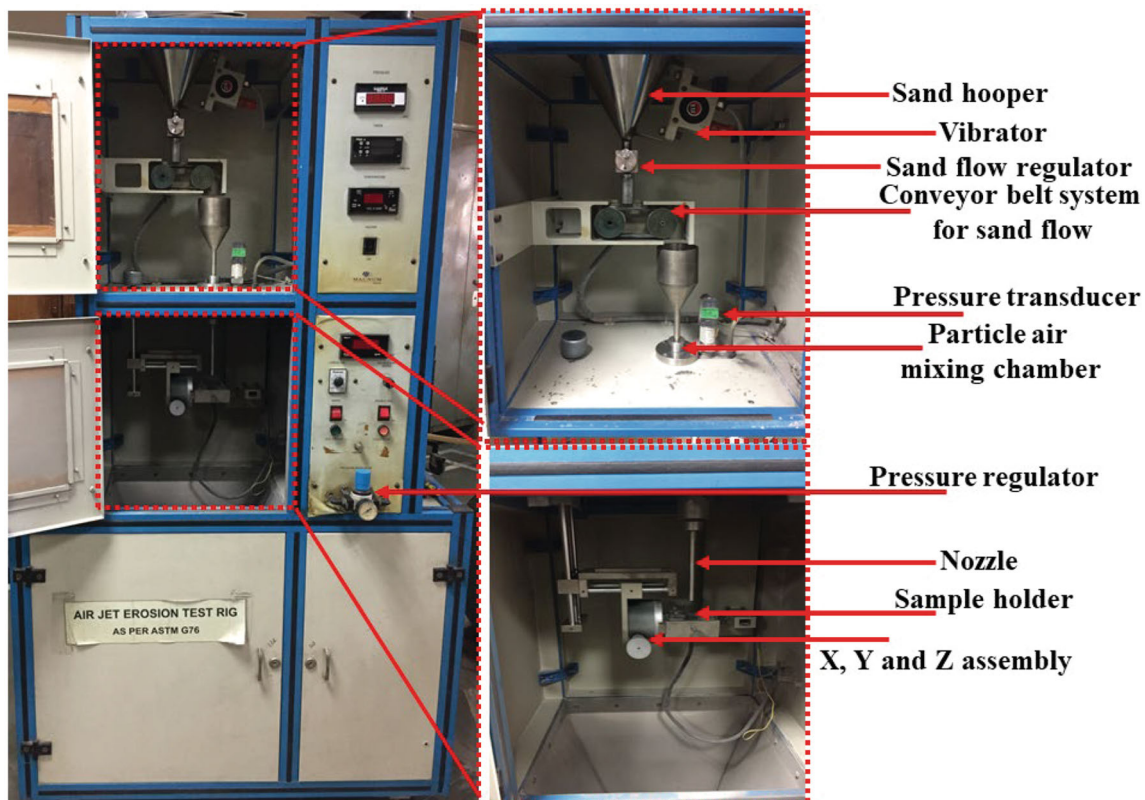


Fig. 1 Air jet erosion test rig

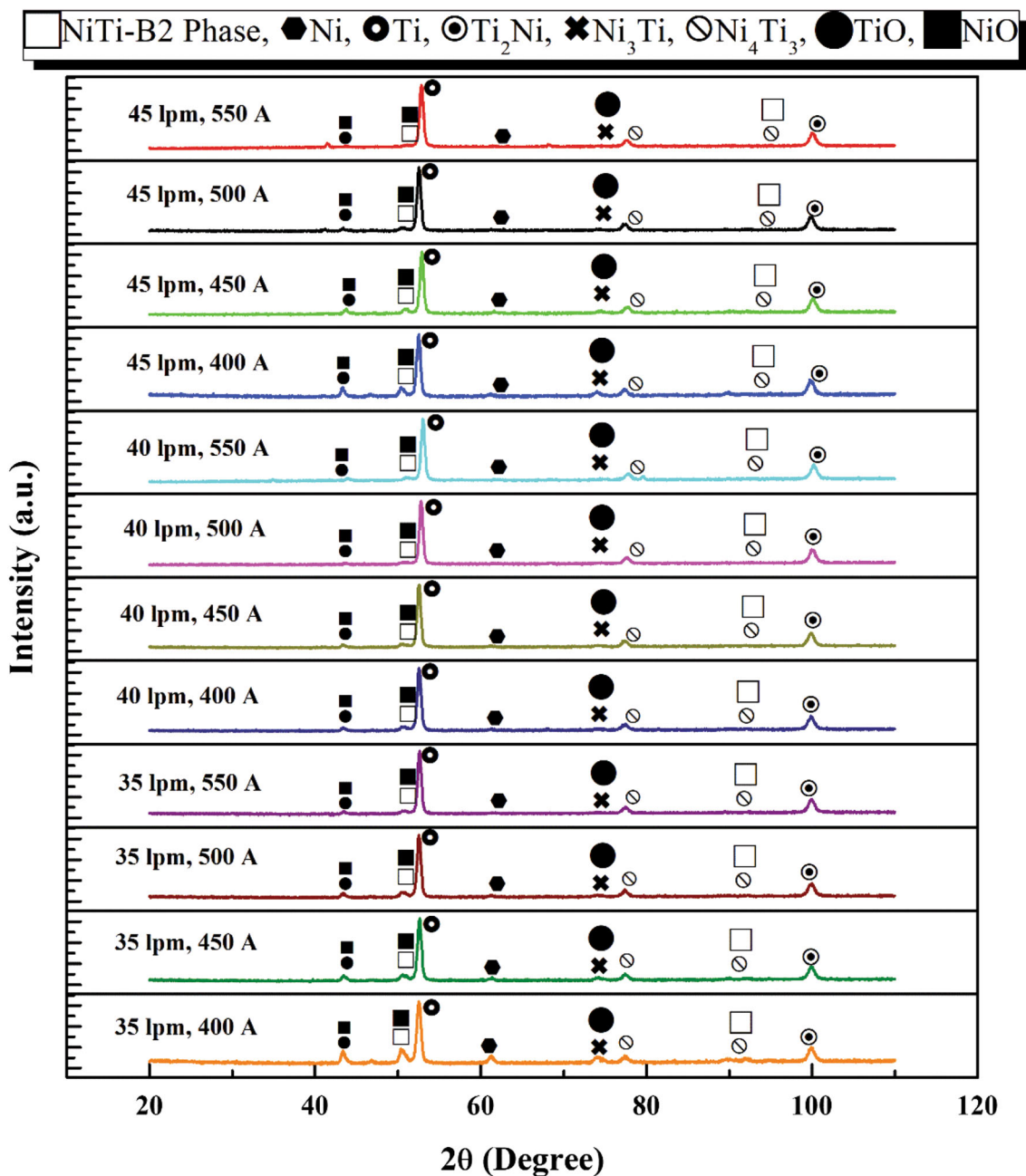


Fig. 2 X-ray diffraction analysis of plasma sprayed NiTi coating

feeder, an air particle mixing and accelerating chamber. The Hooper stores the erosive particles and allows the particles to flow on to the conveyer belt at a particular feed rate. A uniform and continuous flow has been maintained by the help of vibrator equipped alongside the Hooper. The process involves the flow of the mixture (pressurized air and erodent particles) through the nozzle from the conveyer belt to impinge on the targeted material surface.

For the erosion test, silica sand having particle size $200 \pm 50 \mu\text{m}$ and hardness of $1420 \pm 50 \text{HV}$ has been considered as the erodent particle. In the current test, the

abovementioned erodent particles were mixed with dried and compressed air and flowed through a convergent nozzle of internal diameter 1.5 mm and impinging on the surface of the coating. The erodent has been impinged at angles of 45° and 90° , at a pressure of 4 bar and a feed rate of 3 g/min.

Characterizations

The developed coatings have been characterized using scanning electron microscope (SEM) (Make: JEOL 6480LV) attached with energy-dispersive spectroscopy

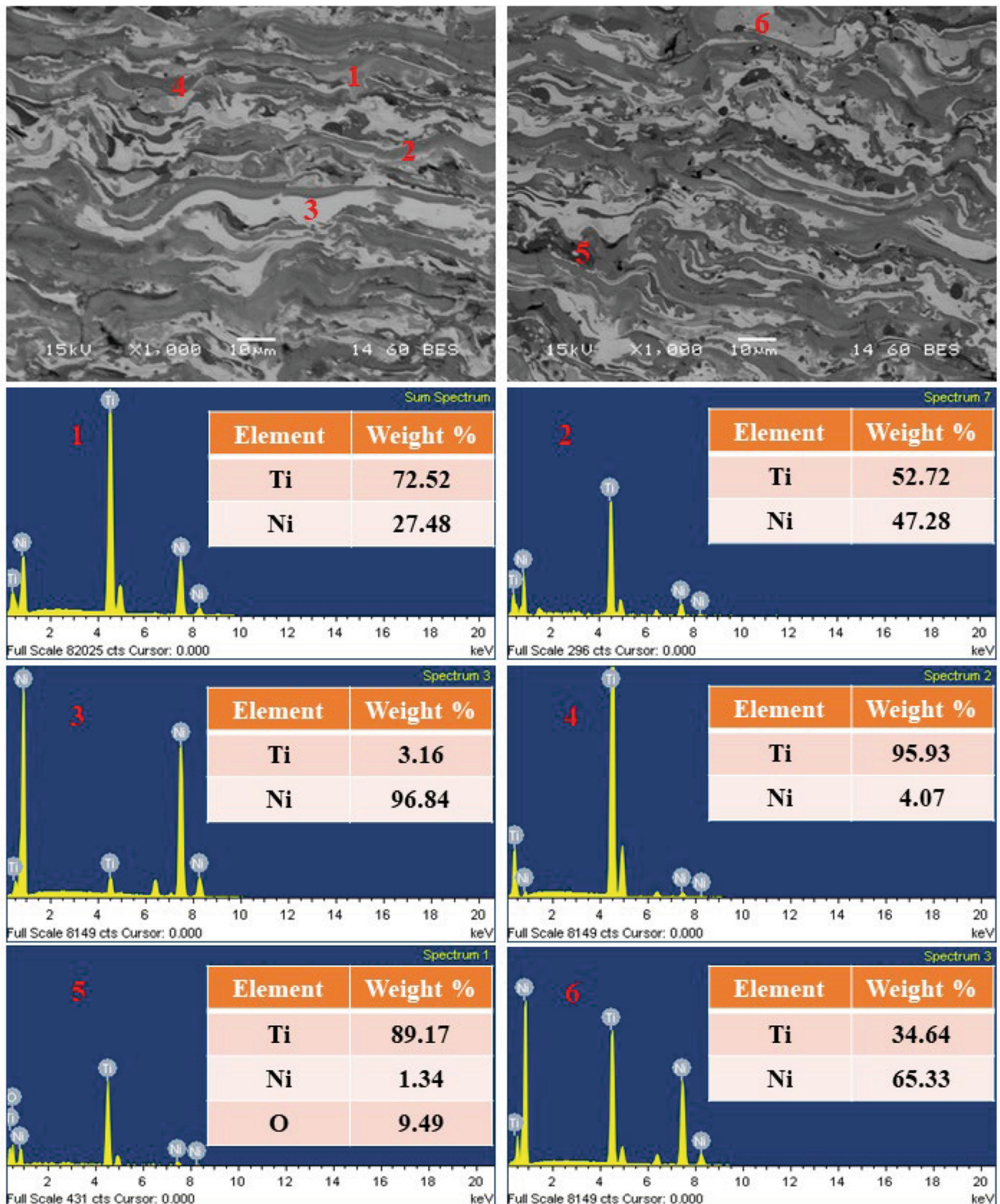
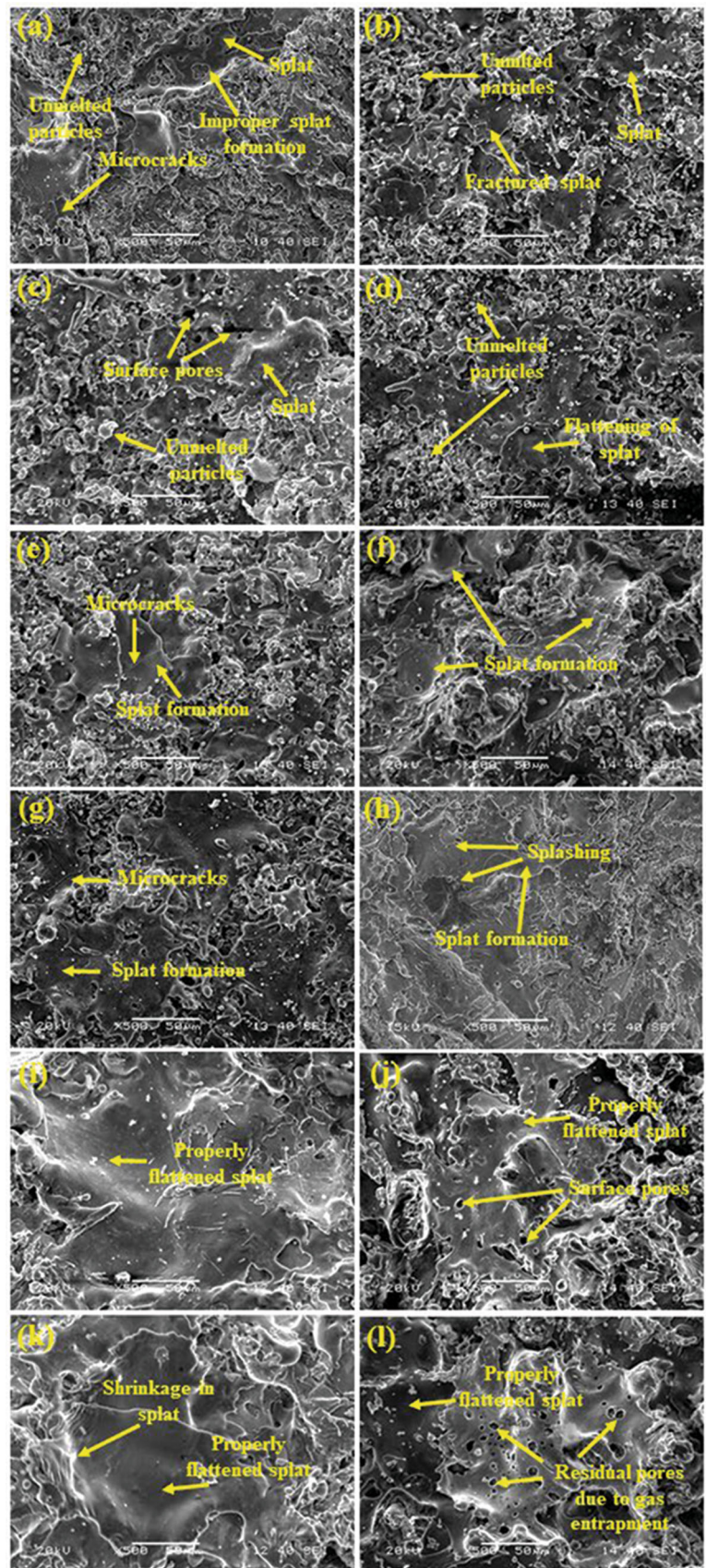


Fig. 3 EDS analysis of plasma sprayed NiTi coating developed at 45 lpm and 550 A

(EDS) for surface and interface morphological analysis and elemental analysis, x-ray diffractometer (XRD) (Make: Contour GT-K Bruker, USA) for phase analysis, stylus

surface profilometer (Make: Veeco dektak 150) attached with Leica DM microscope for surface roughness measurement. In addition to the above, the microhardness and

Fig. 4 Surface morphology of NiTi plasma sprayed coating (a) 35 lpm, 400 A, (b) 35 lpm, 450 A, (c) 35 lpm, 500 A, (d) 35 lpm, 550 A, (e) 40 lpm, 400 A, (f) 40 lpm, 450 A, (g) 40 lpm, 500 A, (h) 40 lpm, 550 A, (i) 45 lpm, 400 A, (j) 45 lpm, 450 A, (k) 45 lpm, 500 A, (l) 45 lpm, 550 A



porosity have been determined using ASTM-E384 and ASTM E2109-01 (2014), respectively. The adhesion strength of the developed coatings has been evaluated by the ASTM-C 633 standard (Ref 46).

Experimental Uncertainties

For the quantification error, all the experiments and measurements were conducted thrice and the average values were reported. Before the measurement, each measuring instrument was calibrated, and after ensuring a maximum error of less than 1%, the measurements were conducted. All the measurement and characterizations follow the protocols reported in ASTM standards.

3.1 Characterization of Plasma Sprayed NiTi Coating.

X-ray Diffraction Analysis

The x-ray diffraction analysis of the plasma sprayed NiTi coating (Fig. 2) revealed the formation of various phases like NiTi-B2 phase, Ni₃Ti, Ti₂Ni, Ni, Ti, NiO, TiO and Ni₄Ti₃. The NiTi-B2 phase is the high temperature parent phase of the NiTi alloy that consists of a cubic crystal structure. This phase belongs to the Pm-3 m space group and formed when Ni content increases. This phase is responsible for the martensitic transformation and shape memory effect (Ref 47). The properties of the phase includes Young's modulus of 75-83 GPa, yield strength of 195-690 MPa and thermal expansion coefficient of $11 \times 10^{-6}/^{\circ}\text{C}$ (Ref 48). The pure Ni and Ti phases were formed as the elemental mixture of Ni and Ti powder has been considered as the feedstock material. The oxide phases like NiO and TiO are formed due to the development of the coating in the open atmosphere. The formation of Ni₃Ti and Ti₂Ni is due to the eutectoidal decomposition of NiTi matrix. In addition to the above, from the comparison of XRD patterns, no significant variation in the formed phases has been observed. However, there are little variations in peak intensities can be noticed. These variations are expected due to the inhomogeneity in coating or intercalation of foreign atoms or variation in crystallite sizes. The abovementioned phases have been confirmed from the EDS analysis (Fig. 3) of the coating.

Surface Microstructural Investigation

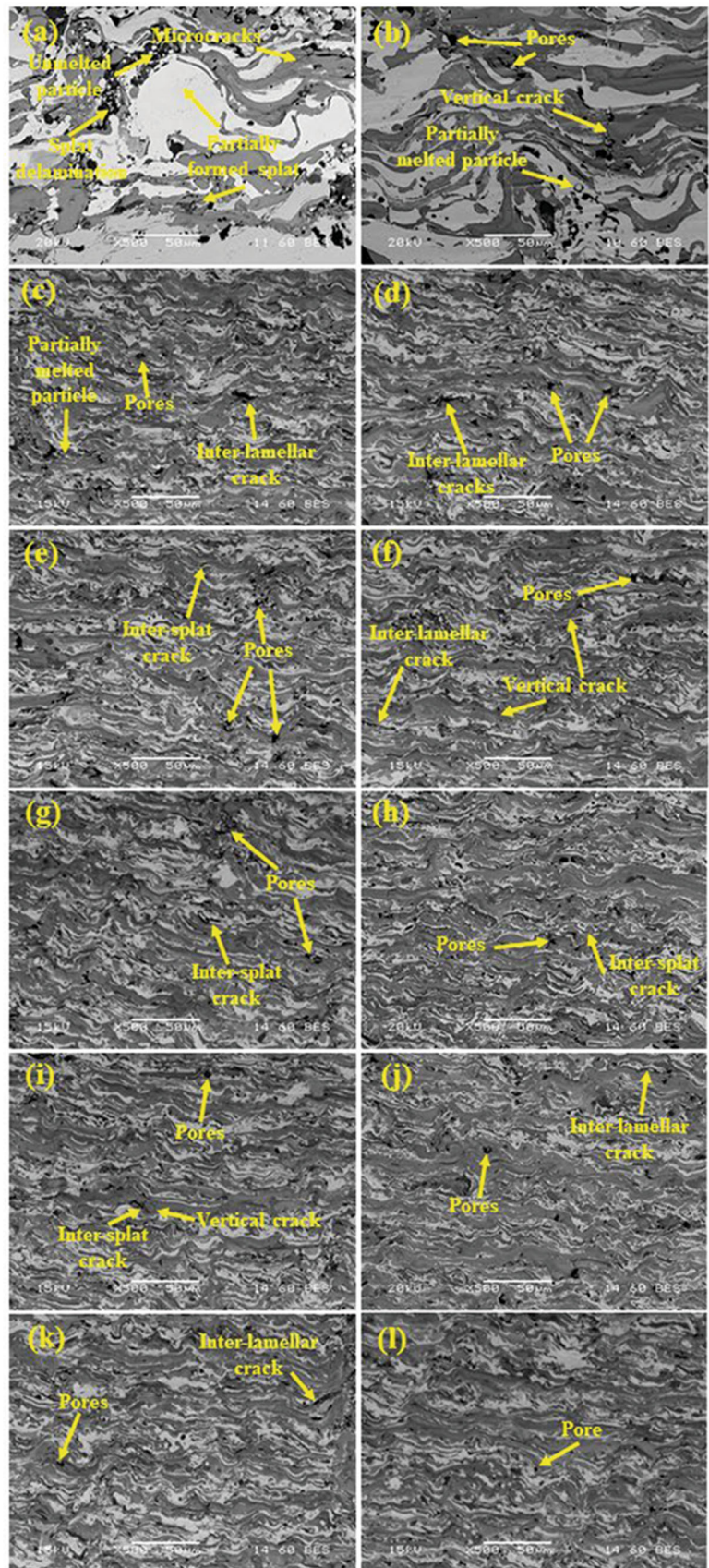
Figure 4 depicts the surface micrographs of the atmospheric plasma sprayed NiTi coatings developed at different primary gas flow rate and plasma arc current. It can be noticed that at lower primary gas flow rate and plasma arc

current, there are various coating defects present in the surface. These defects include surface microcracks, unmelted/partially melted particles, surface pores, splat fracture, etc. The enhancement in the formation of surface microcracks is due to the sudden cooling after coating formation. Again, some literature also reported that these microcracks formation is due to the mismatch in coefficient of thermal expansion of substrate and coating materials (Ref 49). Furthermore, at lower primary gas flow rate and plasma arc current due to the absence of sufficient heat transfer to the powder particles, the proper melting and flattening behavior cannot be expected. Due to the above-mentioned phenomenon, the powder particles cannot be deposited well and remain unmelted or partially melted on the coating surface and hampers the coating properties significantly. In addition to the above, at lower primary gas flow rate and plasma arc current, the temperature and velocity of the particles are low which leads to the delay in reaching the particles on the substrate. As a result, the interference time of the surrounding gases is more. Due to this interference of the surrounding gases, the temperature of the particles is reduced by the convective heat transfer and this results in the formation of unmelted or partially melted particles. In addition to the above surface defects, the surface porosity is one of the major defects which affect the properties of the coating. The formation of surface porosity is due to the presence of unmelted particles formation (Ref 50) or the effect of residual stresses (Ref 51). At lower primary gas flow rate and plasma arc current, the unmelted particles are mainly responsible for the porosity formation, and at higher primary gas flow rate and plasma arc current, the residual holes due to gas entrapments are responsible for the surface pores. Splat fractures are mainly due to the residual stresses present in the coating or the coefficient of thermal expansion mismatch or the presence of the foreign particles in the feedstock material.

Interface Microstructural Investigation

Figure 5 illustrates the cross-sectional view of the NiTi plasma sprayed coatings developed at different gas flow rates and different plasma arc currents. It can be noticed that as the gas flow rate and plasma arc current increases, more homogenized and layered splats have been formed. The abovementioned phenomenon is due to the proper melting and deposition of layer-by-layer structure of the splats with increase in primary gas flow rate and plasma arc current. The coatings developed at low plasma arc current and primary gas flow rate depict various coating defects such as porosity, inter-lamellar cracks, vertical cracks, and inter-splat cracks. Various literature works have been reported the information about the porosity formation of plasma spray coatings. Some researchers have reported that

Fig. 5 Surface morphology of NiTi plasma sprayed coating (a) 35 lpm, 400 A, (b) 35 lpm, 450 A, (c) 35 lpm, 500 A, (d) 35 lpm, 550 A, (e) 40 lpm, 400 A, (f) 40 lpm, 450 A, (g) 40 lpm, 500 A, (h) 40 lpm, 550 A, (i) 45 lpm, 400 A, (j) 45 lpm, 450 A, (k) 45 lpm, 500 A, (l) 45 lpm, 550 A



the formation of porosity is due to the interaction of the particles with the gaseous medium, splashing on the impingement on the substrate or pre-deposited splat and partially molten particle deformation (Ref 52). Other researchers have reported that the pores are formed due to the entrapped gases, partially filling in solidifying splats and shrinkage in splat due to rapid solidification (Ref 53–55). The inter-lamellar crack formation occurs when the crack resistance at splat interface and grain boundary is higher than the lamellar interface (Ref 56), and inter-splat pores or inter-splat microcracks are formed due to the improper bonding between two consecutive splats or due to the effect of oxide formation. Sometimes, the vapors generated from the chemical reactions are entrapped with some inclusions or unmelted particles and amalgamate during solidification process (Ref 57). The abovementioned phenomenon leads to the formation of voids. In some cases, these voids induce coating delamination and formation of inter-lamellar microcracks (Ref 58). In addition to the above defects, the vertical microcrack formation has also

been observed from the interface morphology of the plasma sprayed coating. These vertical microcracks are expected to form due to the increase in residual stress by the virtue of thermal mismatch between coatings (Ref 59). Furthermore, the hotter plasma and stronger surface cooling enhances the temperature gradient during the transient cooling, and this also leads to the formation of vertical microcracks (Ref 60).

Porosity Analysis

Figure 6 illustrates the variation in porosity with respect to the plasma arc current and primary gas flow rate. It can be observed that with the increase in primary gas flow rate and plasma arc current, the porosity percentage of the coatings decreases. In plasma spray coating process, the powder particles are gone through the plasma plume in molten/semi-molten state and finally deposited on the substrate or previously deposited splats and build a layer-by-layer splat formation. This process continues until certain coating

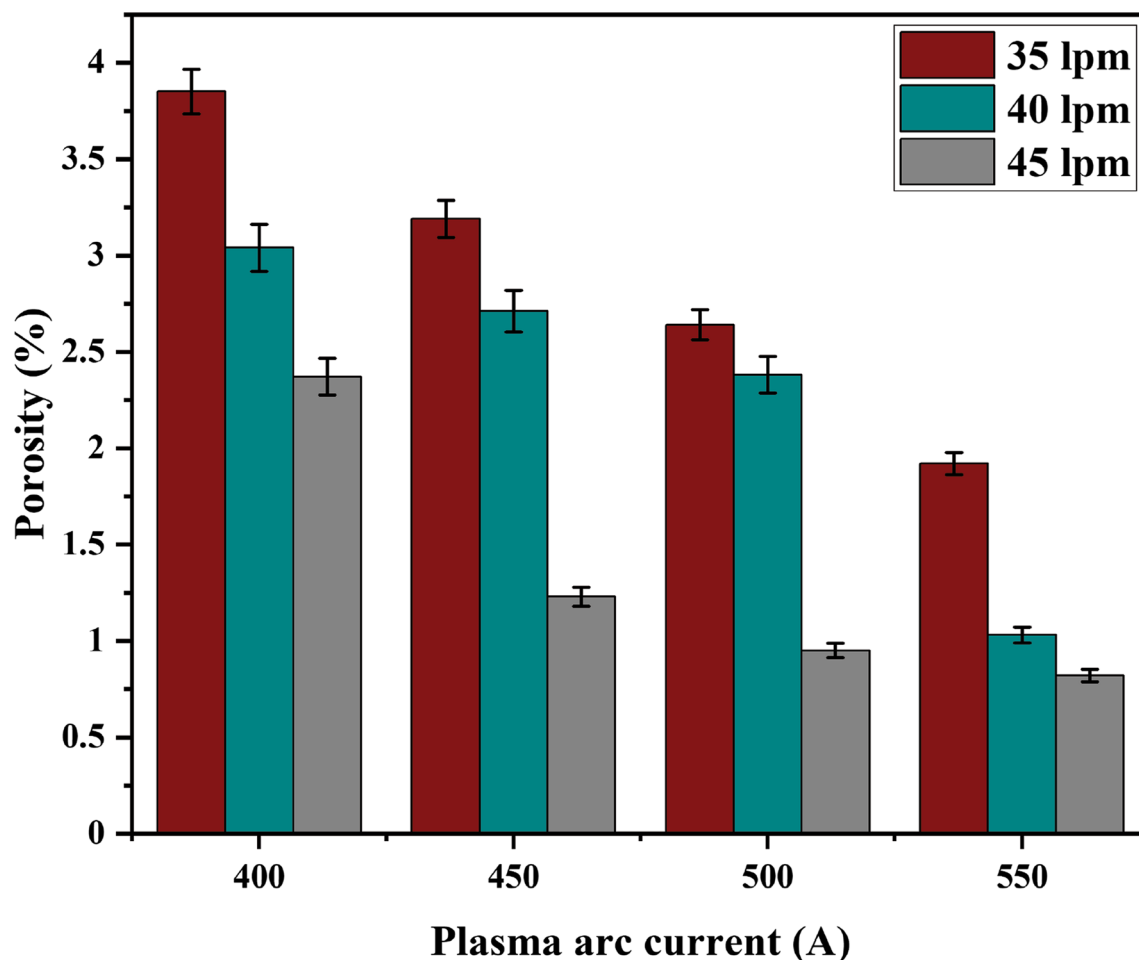


Fig. 6 Variation in porosity with primary gas flow rate and plasma arc current

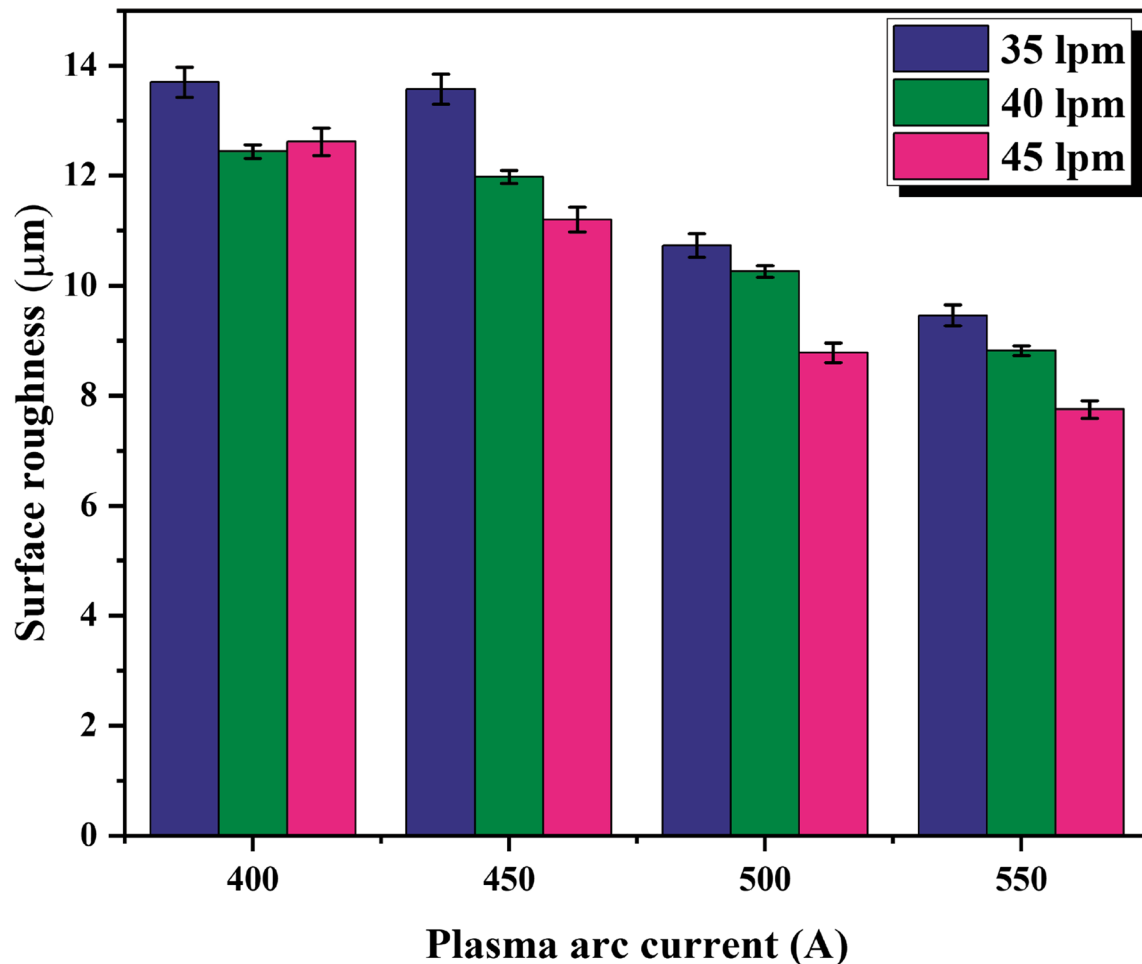


Fig. 7 Variation in surface roughness with plasma arc current and primary gas flow rate

thickness has been achieved. The quality of the plasma spray coating depends on the adhesion/cohesion bond formed between substrate/coating or within the buildup layers. The effect of high temperature leads to the inter-diffusion from the underlying compacted layers and forms the splat after solidification by interlocking mechanism. The presence of entrapped airs, voids and unmelted particles within the layers leads to the formation of pores of various shapes and sizes (Ref 61). Basically, porosity forms due to the entrapped gases and solidification shrinkage (Ref 62, 63). The porosity is developed when the gap between the pre-deposited splats is not overlaid by the subsequent splats. At lower primary gas flow rate and plasma arc current, due to the more interaction time of the particles with the surrounding gases, the chances of gas entrapment are more. Furthermore, at lower primary gas flow rate and

plasma arc current, the temperature and velocity of the in-flight particles are less which leads to the formation of more unmelted particles and voids. Therefore, at lower primary gas flow rate and plasma arc current, the amount of porosity percentage is more.

Surface Roughness Analysis

Figure 7 represents the variation in surface roughness with the primary gas flow rate and plasma arc current. It can be observed that the surface roughness of the coating decreases with increase in plasma arc current. At lower arc current, the powder particles experience the less enthalpy which leads to the improper heat transfer to the particles. Due to the abovestated phenomena, the melting of the particle cannot be proper. This leads to the formation of

unmelted particles deposition on the substrate or pre-deposited splats. This phenomenon creates inhomogeneity in the coating and ultimately creates a coating with high roughness. Furthermore, at lower plasma arc current, the time to gas entrapment is more, which creates more residual holes on the surface. As a result, the surface roughness of the coating increases. According to the literature (Ref 64), the length of the plasma column depends on the primary gas flow rate. It means, the increase in primary gas flow rate increases the length of the plasma column. The abovementioned phenomenon enhances the melting fraction of the particles and restricts the bad effects on the properties of the coating. Furthermore, increase in primary gas flow rate leads to the increase in particle velocity as the particle velocity depends on the working mass flow rate of the primary gas. This phenomenon leads to the decrease in surface roughness of the coating. The roughness profiles of the coatings are illustrated in Fig. 8.

Microhardness Evaluation

The variation in microhardness with the plasma arc current and primary gas flow rate is illustrated in Fig. 9. It indicates the increasing behavior of the microhardness with the plasma arc current and primary gas flow rate. The increase in primary gas flow rate and plasma arc current leads to an enhanced flattening ratio and molten degree of the particle. The abovementioned phenomenon reduces the porosity percentage of the coating and ultimately enhances the hardness value of the coating. In addition to the above, the effect of thermal pinching on the particle impact velocity is significant. The increase in primary gas flow rate increases the chances of thermal pinching effect which leads to the enhancement in particle velocity and a denser deposition has been achieved. This leads to the enhancement in the microhardness. Furthermore, the lower plasma arc current results in lower plasma plume which leads to insufficient heat transfer and formation of a coating having various surface defects like pores, voids, microcracks, unmelted particles, etc. These defects reduce the microhardness value of the coating. Again, at lower plasma arc current, the enthalpy of the plasma plume is low which results in insufficient heat supply to the powder particles. These phenomenon encourages the formation of unmelted/ or partially melted particles and ultimately reduces the microhardness value of the coating.

Bond Strength Evaluation

Figure 10 illustrates the variation in adhesion strength with the process parameters, such as primary gas flow rate and plasma arc current. It can be observed that the adhesion strength increases with the increase in primary gas flow rate. This is due to the enhancement in residence time of the particle and particle melting ratio resulted by the enhancement in plasma column length. Furthermore, the increase in ionization process leads to the decrease in formation of unmelted particles. As a consequence, a coating with better adhesion strength has been achieved. In addition to the above, the rise in available energy at higher plasma arc current increases the enthalpy of the plasma plume. As a result, a coating with better molten fraction has been formed. This enhances the adhesion strength of the coating. Very high plasma arc current leads to the entrapment of the gas in the splat. The abovementioned phenomenon reduces the adhesion strength of the coating.

Solid Particle Erosion Performance Evaluation

Relation Between Microstructure and Phase with Erosion Behavior of the Plasma Sprayed NiTi Coating

From the microstructural analysis, various surface defects have been noticed in the developed coatings. These surface defects also affect the erosion performance of the coating. The observed defects are unmelted particles formation, fractured splats, microcracks, surface pores, etc. The presence of microcracks, fractured splats and surface pores leads to the easier penetration of the erodent in the coating surface and damages the coating. The erodent intensifies the surface defects after impingement. The presence of unmelted particles sometimes becomes advantages and sometimes disadvantages for the coating in erosion environment. The presence of unmelted particles creates roughness by virtue of which the erodent particles retard and resulted in less mass loss of the coating. In the same time, the presence of unmelted particles creates porosity and improper adhesion/interfacial bond and resulted in more mass loss after erodent impingement. Richman et al. (Ref 65) stated that the austenitic phase NiTi-B2 has a higher erosion resistance due to the superelasticity property and the accumulation of little strain. In addition to the above, the formation of intermetallics like NiTi, Ti₂Ni and

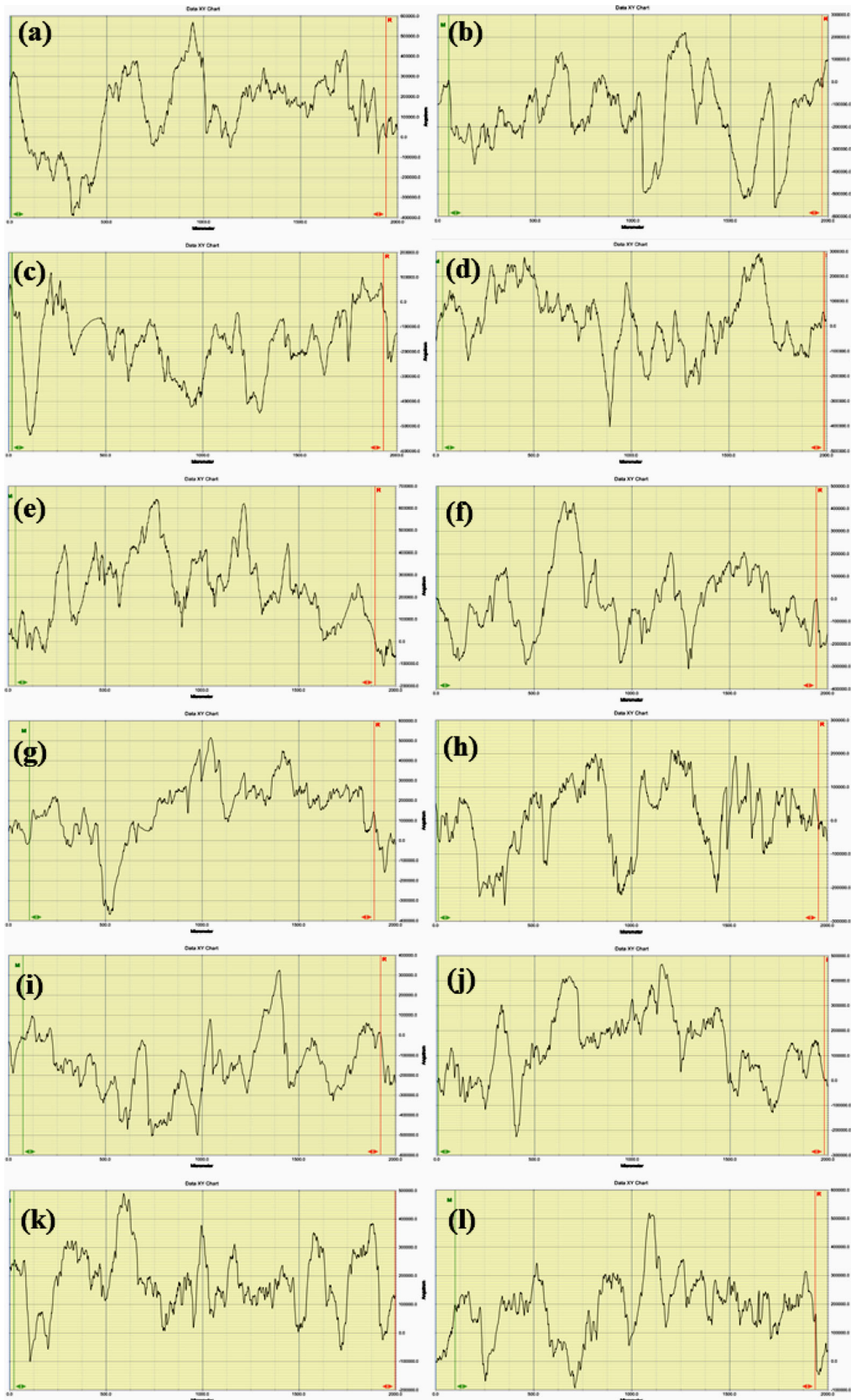


Fig. 8 Surface roughness of NiTi plasma sprayed coating (a) 35 lpm, 400 A, (b) 35 lpm, 450 A, (c) 35 lpm, 500 A, (d) 35 lpm, 550 A, (e) 40 lpm, 400 A, (f) 40 lpm, 450 A, (g) 40 lpm, 500 A, (h) 40 lpm, 550 A, (i) 45 lpm, 400 A, (j) 45 lpm, 450 A, (k) 45 lpm, 500 A and (l) 45 lpm, 550 A

microhardness and surface roughness. However, the porosity of a thermal spray coating plays a vital role in the erosion property evaluation which cannot be excluded. Figure 11 and 12 indicate the variation in erosion rate of

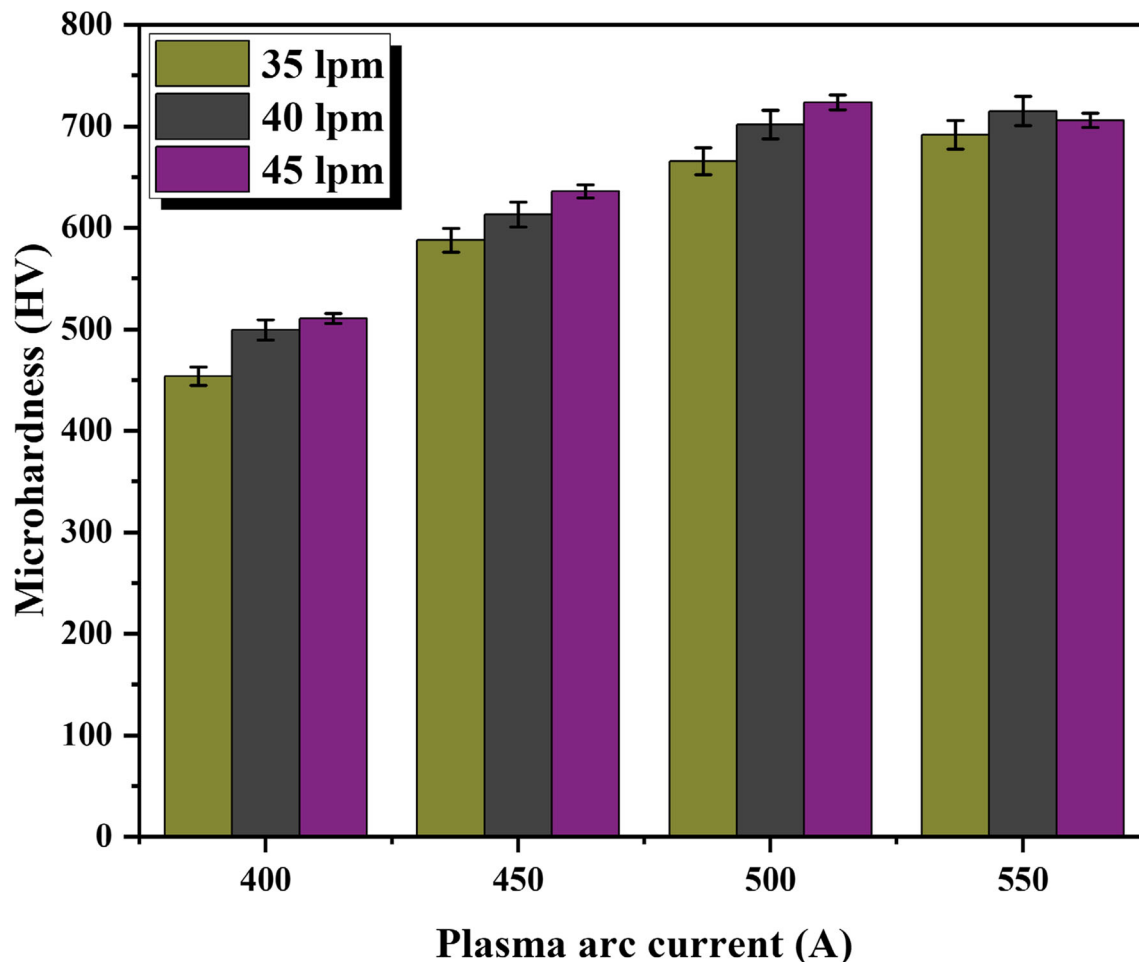


Fig. 9 Variation in microhardness with primary gas flow rate and plasma arc current

Ni₃Ti resulted in enhancement in microhardness value of the coating. Among these intermetallics, the Ti₂Ni phase contributes more toward the microhardness enhancement (Ref 35). Therefore, the abovementioned phases also contribute to the erosion performance of the coating.

Relation Between Porosity and Erosion Rate of The plasma Sprayed NiTi Coating

It is well known that the erosion rate of the thermal spray coatings depends upon the various parameters such as

the samples eroded at erodent angles 45° and 90° impingement angle with the porosity percentage. It can be observed that the erosion rate of the coatings increases with increase in porosity percentage in both the erodent angles (45° and 90°) of impingements. This is due to the decrease in material strength against the plastic deformation or chipping, which is resulted due to the lack of mechanical support at the edge of the voids/pores. When the erodent particles strike the surface of the coating having porosity, the edges of the voids are the part of the coatings which is removed or damaged quickly as compared to the plane

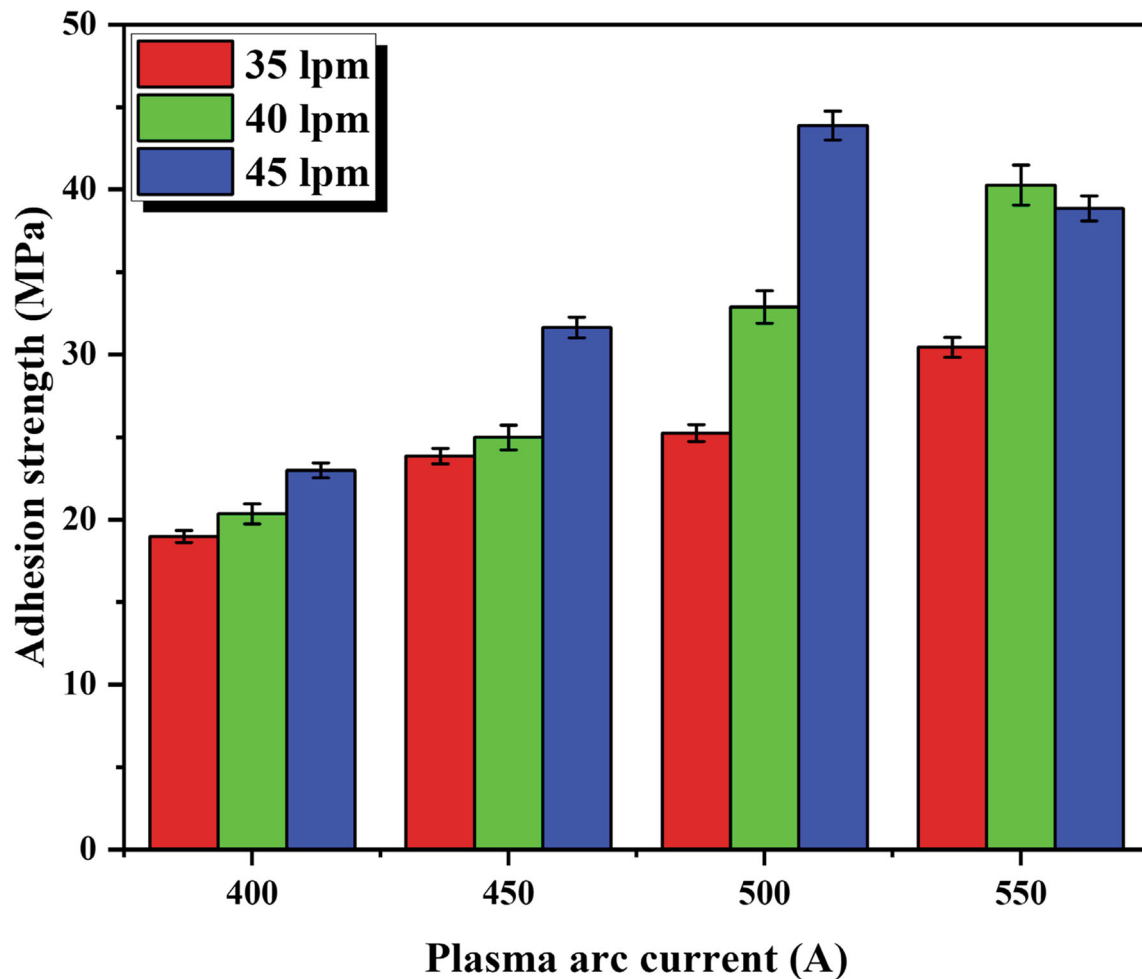


Fig. 10 Variation in adhesion strength with primary gas flow rate and plasma arc current

surface. However, the abovementioned phenomenon happens different in the different particle impingement angles. When the erodent particles strike at an angle of 45° at the edges of the voids, the major component for the material removal is the shear force though both normal and shear forces act at that point. As a result, the outer edge of the voids damages more and the chances of damage of the roots of the voids are very less. The roots are only affected by the abrasion of the erodent (Fig. 13). However, when the erodent particles impinged at the edges of the voids, normally, it damages more than lower angle impingements. The aforesaid is due to the completely removal of the edges of the voids. The abovementioned phenomenon enhances the material removal of the coating and hence the erosion rate. In addition to the above, the erosion at the concave

surface inside a void/pore which is not under the shadow of the void edges, also affects the erosion rate of the coating. The abovementioned area experiences the erodent at an angle higher than the average target surface. Furthermore, according to the literature (Ref 66), the ductile materials erode more at a lower erodent impingement angle and brittle materials erode more at higher impingement angle. Therefore, the concave surface under the shadow of the void edges experiences more damage if it is brittle in nature and less damage is expected if the surface is ductile. Furthermore, the porosity also acts as a stress concentrator, and as a result, the chances of failure at this point increase which leads to the material loss in case of solid particle erosion wear. According to the literature (Ref 45), the erosion phenomenon of the plasma spray coating is also

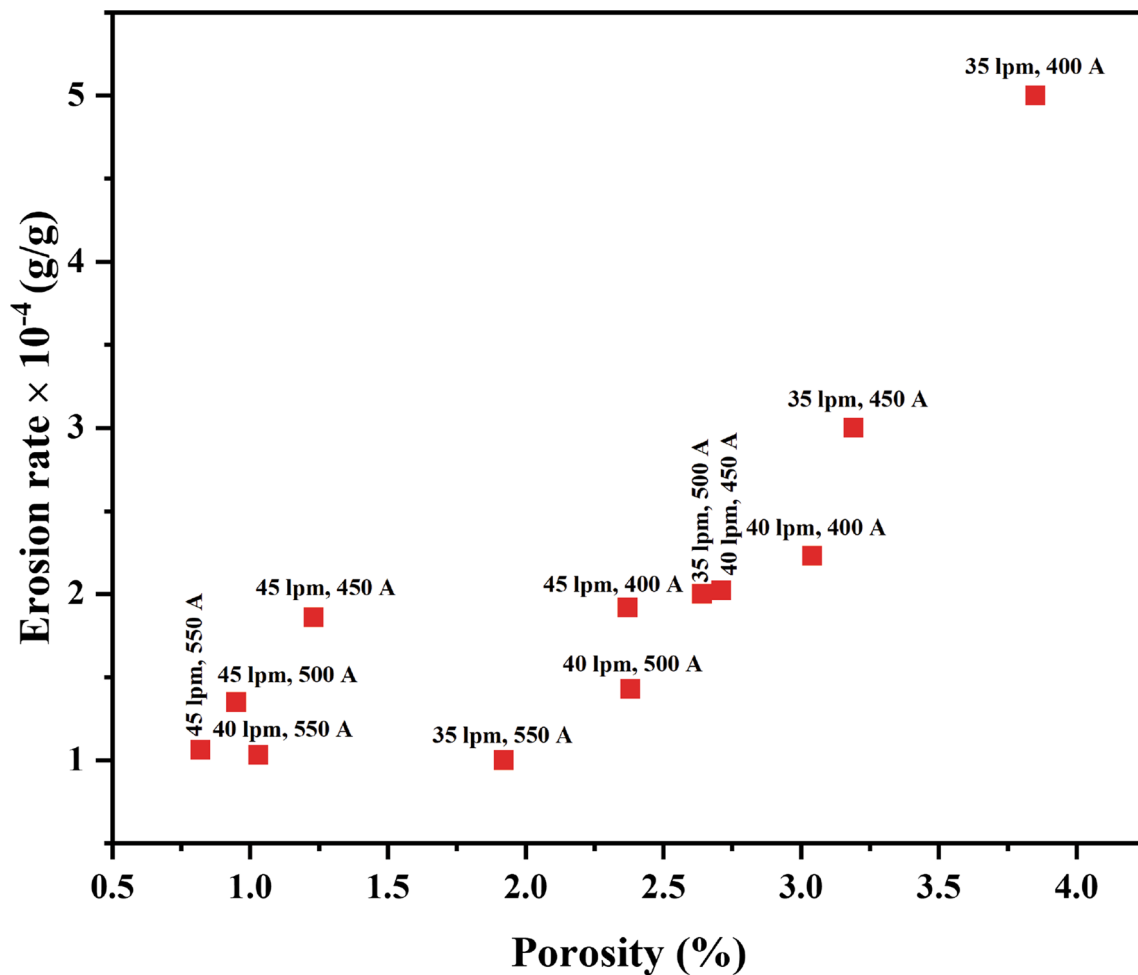


Fig. 11 Relation between porosity and erosion rate of the plasma sprayed NiTi coating with impinging erodent angle of 45°

affected by the crack propagation along the inter-splat boundary. The porosity present at the inter-splat region of the plasma spray coating weakens the adhesion/cohesion force between the splats, and as a result, the damage due to the erosion increases. Hearnly et al. (Ref 67) also reported that the porosity in the inter-splat boundary not only declines the strength or bonding between the splats but also develops microcracks which leads to the damage of the lamellae and hence mass loss from the coating.

Relation Between Surface Roughness and Erosion Rate of the Plasma Sprayed NiTi Coating

Although, the erosion of a plasma spray coating depends upon various phenomena, the effect of surface roughness

cannot be ignored. It can be observed that in most of the cases, the erosion rate of the plasma sprayed coating is higher at higher surface roughness. In case of erodent impingement at an angle of 45° (Fig. 14), at higher surface roughness, the erodent particles have more surface area to damage as compared to the surface having lower surface roughness. When the erodent particle strikes the rough profile of the coating at an angle of 45°, the damage is more when the height of the peak is more. The aforesaid phenomenon involves the concept of damage of the peaks nearer from the roots by the impingement of the erodent at an angle of 45° or reduce the peak heights (Fig. 15). At lower surface roughness, the erodent has less area to damage which leads to lower in mass loss. However, in case of erodent impingement of 90° (Fig. 16), the surface

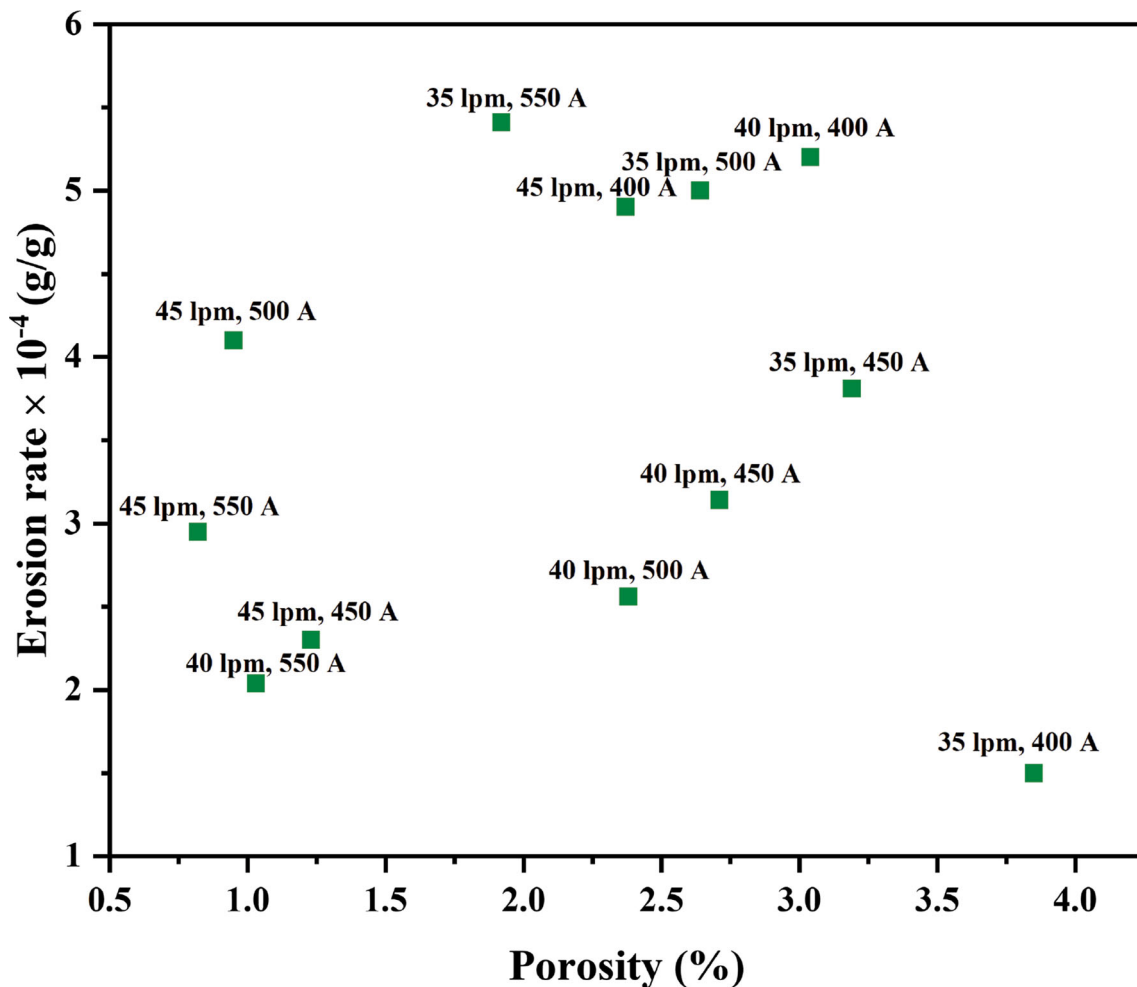


Fig. 12 Relation between porosity and erosion rate of the plasma sprayed NiTi coating with impinged erodent angle of 90

having higher surface roughness erodes more as compared to the surface having lower roughness value because when the erodent particle strikes the surface, normally, it damages more at the space between two roughness peaks due to more stress concentrations and forms deeper grooves (Fig. 17). At the surface having lower roughness, the stress concentration is less, as a result, there are less mass loss carried out. Furthermore, by keeping all the parameters constant, the required impingement velocity of the erodent to penetrate in the coating surface is more for a surface with lower surface roughness. The abovementioned surfaces having lower surface roughness values lead to a lower mass loss during erosion than the surfaces having higher surface roughness (Ref 68) at the erodent impingement of 90°. At some samples, it can be observed

that the erosion wear increases with decrease in surface roughness and vice versa. The reason for the abovementioned is different for the surface impinged at different impingement angles. When the erodent particles strike the coating surface at an angle of 45°, at some cases, the retardation of the particles velocity may occur, and as a result, the erodent cannot damage more coatings which leads to less mass loss and erosion rate. Furthermore, when the erodent particles strike the surface of higher surface roughness at an angle of 90°, at some points, the particles cannot penetrate to a more depth in the surface if the height of the surface profile is more. The aforesaid phenomenon results in the lower mass loss which leads to the lower erosion rate. In addition to the above, the reason behind the abovementioned trend is also due to the dominating effect

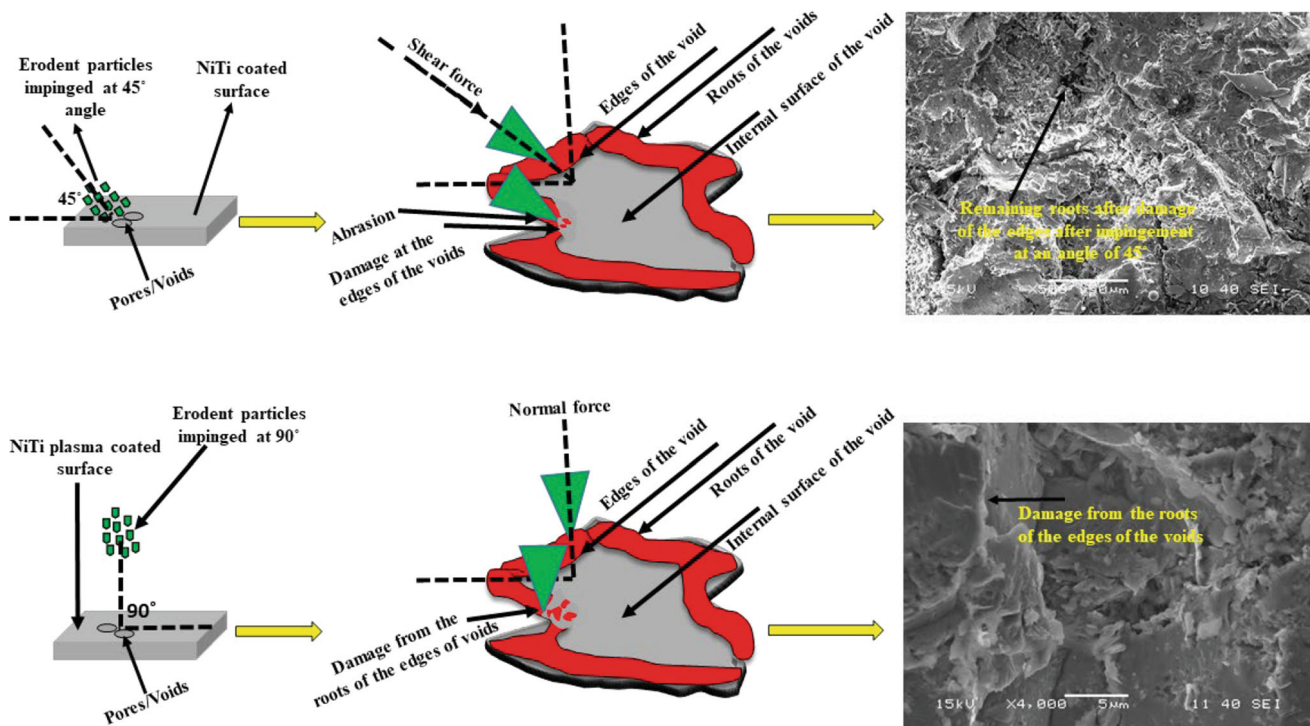


Fig. 13 Schematic and SEM of the damage mechanism at pores of the coating by erodent

of the other influencing parameters on the erosion rate of the plasma spray coating.

Relation Between Microhardness and Erosion Rate of the Plasma Sprayed NiTi Coating

Although there are various parameters affecting the erosion behavior of the plasma sprayed NiTi coating, the effect of hardness cannot be neglected. Figure 18 and 19 reveal the variation in erosion behavior with respect to the microhardness of the coatings impinged at angles of 45° and 90°. It can be observed that the erosion rates of the coatings impinged by both 45° and 90° decrease with increase in hardness values of the coatings. The proposed model by Patnaik et al. (Ref 69) was revealed by the following Equation (Eq 1),

$$E_{th} = \frac{\rho_m \eta U^2 \sin^2 \theta}{2H_v} \quad (\text{Eq 1})$$

where θ is the angle of impingement of the erodent particles (degree) U is the impact velocity (m/s), H_v is the hardness (N/m^2), ρ_m is the density of the material (kg/m^3),

η is the erosion efficiency, E_{th} is the theoretical erosion rate (kg/kg)

According to the abovementioned equation, it can be clearly seen that the erosion rate of the materials is inversely proportional to the hardness. The aforesaid statement has been confirmed by several researchers (Ref 70, 71). Furthermore, the reason behind the aforesaid trend of the graph is the rebound phenomenon of the erodent particles from the coating surface. When the erodent particles strike the coating surface at the angles of 45° and 90°, with an increase in microhardness values, it is expected that some of the erodent particles rebound upon striking the surface. Those erodent particles cannot contribute to the erosion phenomenon of the coating. In addition to the above, in some of the samples, the erosion rate increases with increase in the microhardness values. In those cases, the pseudoelastic property of the NiTi alloy is expected to come into the effect. For those cases, when the erodent particle strikes the coating surface, due to the pseudoelastic property, the material restricts the plastic deformation and regains its shape after removing the external stimuli (force exerted by the erodent particle on the surface). The

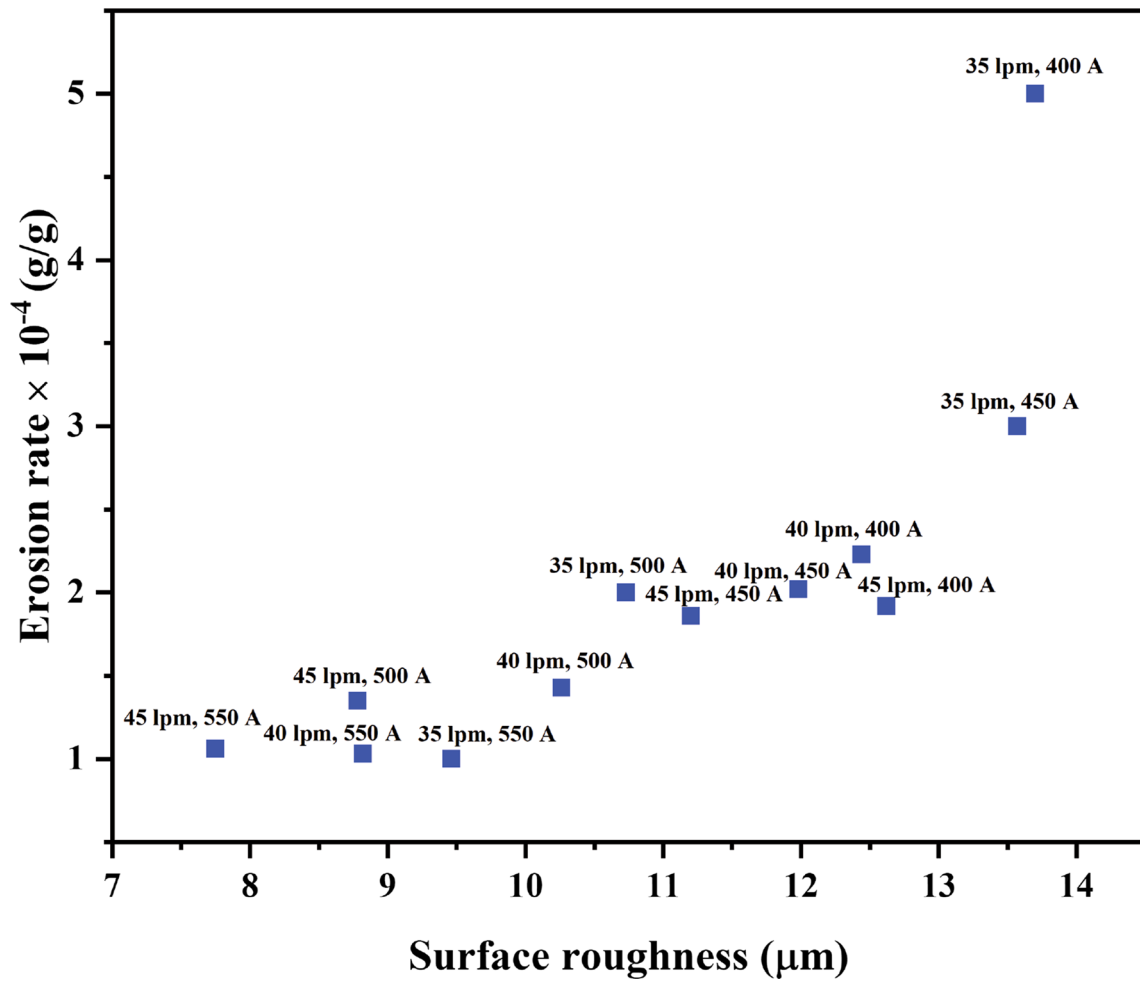


Fig. 14 Relation between surface roughness and erosion rate of the plasma sprayed NiTi coating with impinged erodent angle of 45°

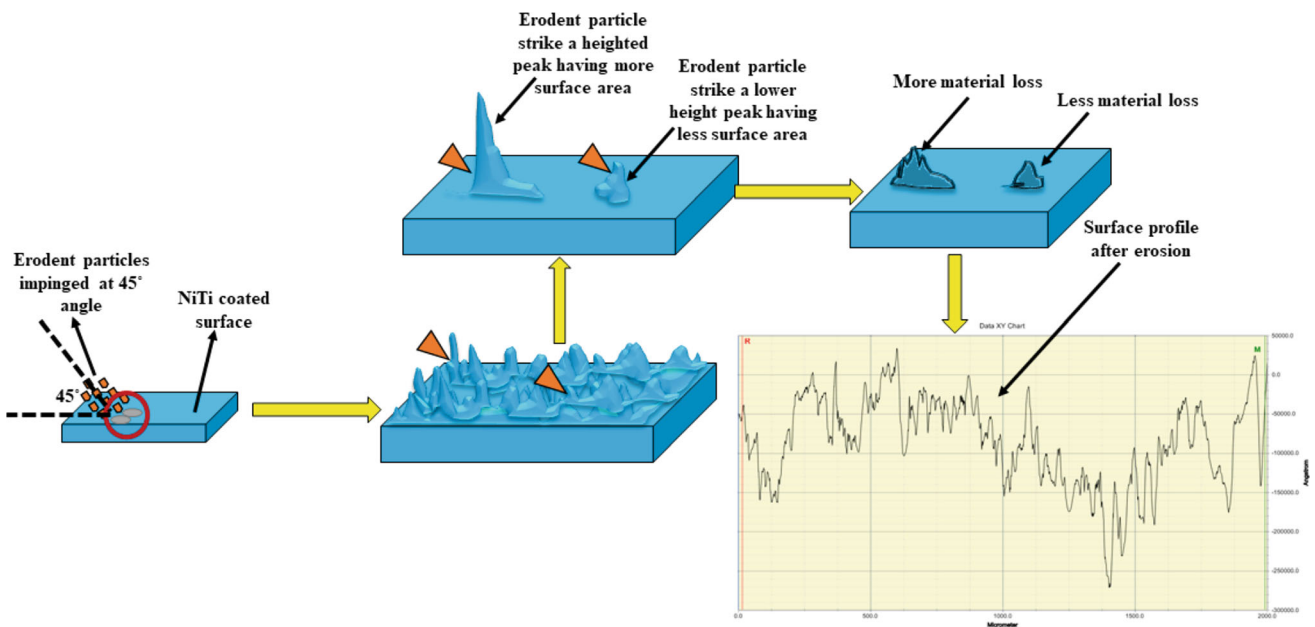


Fig. 15 Schematic of the erosion mechanism and roughness profile of the coating after erosion by the erodent impinged at 45°

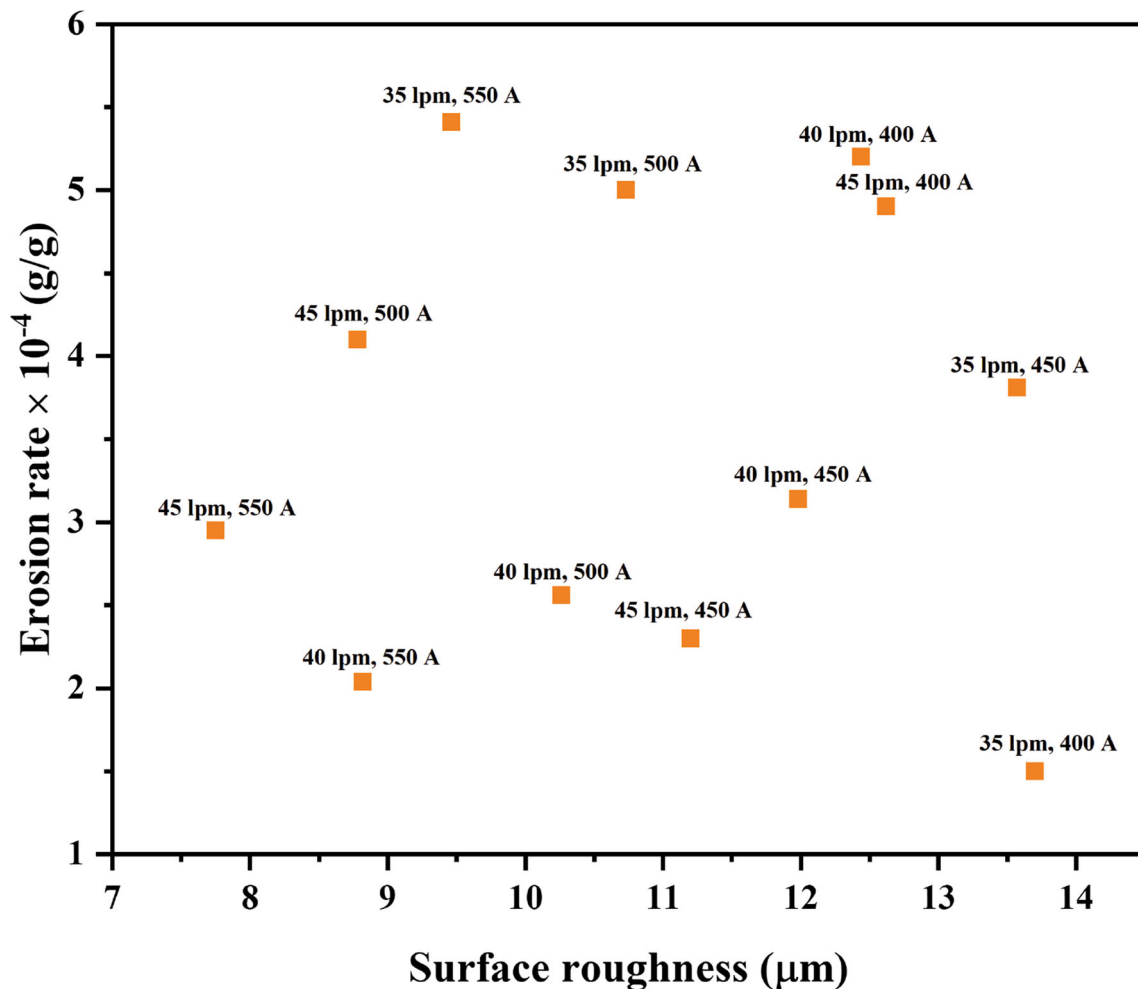


Fig. 16 Relation between surface roughness and erosion rate of the plasma sprayed NiTi coating with impinged erodent angle of 90°

abovementioned phenomenon reduces the mass loss and finally the erosion rate even in a coating having low hardness. Moreover, the increase in erosion rate by increasing hardness is resulted due to the effect of other dominating factors.

Relation Between Erodent Impact Angle and Erosion Rate of the Plasma Sprayed NiTi Coating

Angle of impingement or impact angle plays a significant role in the solid particle erosion wear phenomenon. The impact angles decide the nature of surface, i.e., ductile or brittle. According to Maozhong et al. (Ref 72), there is a relation between erosion rate and impact angle,

$$E = A \cos^2 \alpha \sin(m\alpha) + B \sin^2 \alpha$$

where m , A and B are constants. In the case of brittle material, A is equal to zero and the erosion rate is largest at 90° impact angle. In the case of plastic material, B is equal to zero and the erosion rate is largest at 20–30° impact angle.

In the current work, it can be observed from Fig. 20 that the erosion rate decreases gradually with increase in gas flow rate and plasma arc current in the coating impinged at 45° impingement angle. The abovementioned trend of the graph indicates that with increase in gas flow rate and plasma arc current, the brittleness of the coating increases. However, the same has not been observed in case of 90° impingement angle. At some cases, the erosion behavior

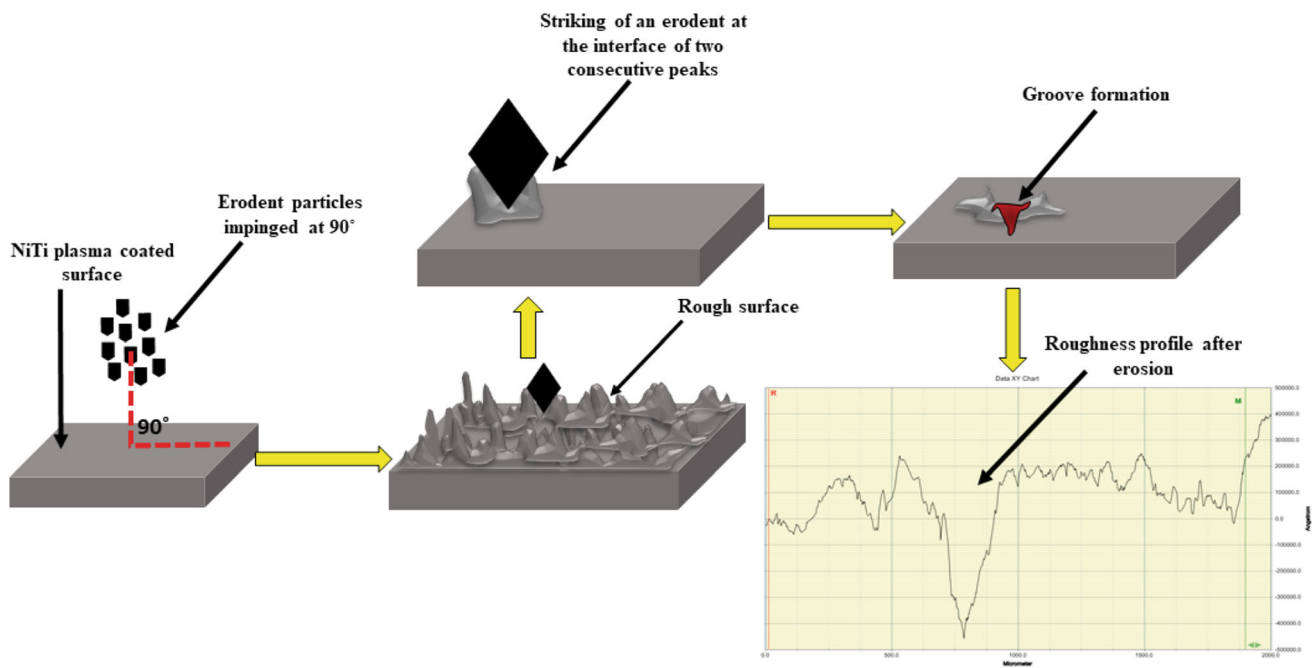


Fig. 17 Schematic of the erosion mechanism and roughness profile of the coating after erosion by the erodent impinged at 90°

differs. This is because the dominating effect of other influencing parameters on the erosion. Furthermore, the maximum erosion rate of the coating has been observed in the erodent impinged at 90° impact angle (Fig. 21). The reason of this type of behavior is the brittle nature of the coating. The surface having the ductile nature basically reveals plastic deformation and microplowing as its erosion mechanisms. Therefore, in these types of erosion mechanisms, the surface is deformed but the chances of removal of the material are less. However, in the case of brittle surfaces, the chances of material removal due to microcutting and groove formation are more. From the above investigation, it can be expected that the coating is of brittle in nature.

Eroded Surface Morphological Analysis

In the erosive conditions, the material removal mechanisms are indicated by the type of surface behaviors, i.e., ductile or brittle. The surface having ductile in nature depicts the mechanisms like cutting and deformation. At the same time, the surface having brittle nature reflects the mechanisms like cracking, chipping, fracture, etc. (Ref 73-75).

Figure 22 illustrates the surface morphologies of the eroded coating surfaces. It can be noticed that the coating impacted at an angle of 90° (Fig. 22a and b) indicates the mechanisms like groove formation, splat fracture, splat fragmentation, splat delamination, pit formation, etc. Furthermore, the surface impinged at 45° erodent impingement angle (Fig. 22c and d) depicts the erosion mechanisms like plastic deformation, plowing, microcutting, lip formation, scratches, groove formation, etc. In case of the surface impinged at 45° , the material removal process initiates with plastic deformation and later on by the repeated impingement of the erodent particles more amount of materials have been removed (Ref 76, 77). Furthermore, the formation of lips and ridges is observed at the bank of the grooves, and these lips are eradicated from the surface by further impingement of the erodent. The microcutting/cutting on the coating surface is due to the dominant effect of the horizontal component of the erodent kinetic energy at lower impingement angle. Furthermore, the high impact energy of the erodent leads to the formation of scratches or grooves on the surface. However, in case of the coating impinged at 90° impingement angle, deep cutting or deep groove formation occurs due to the

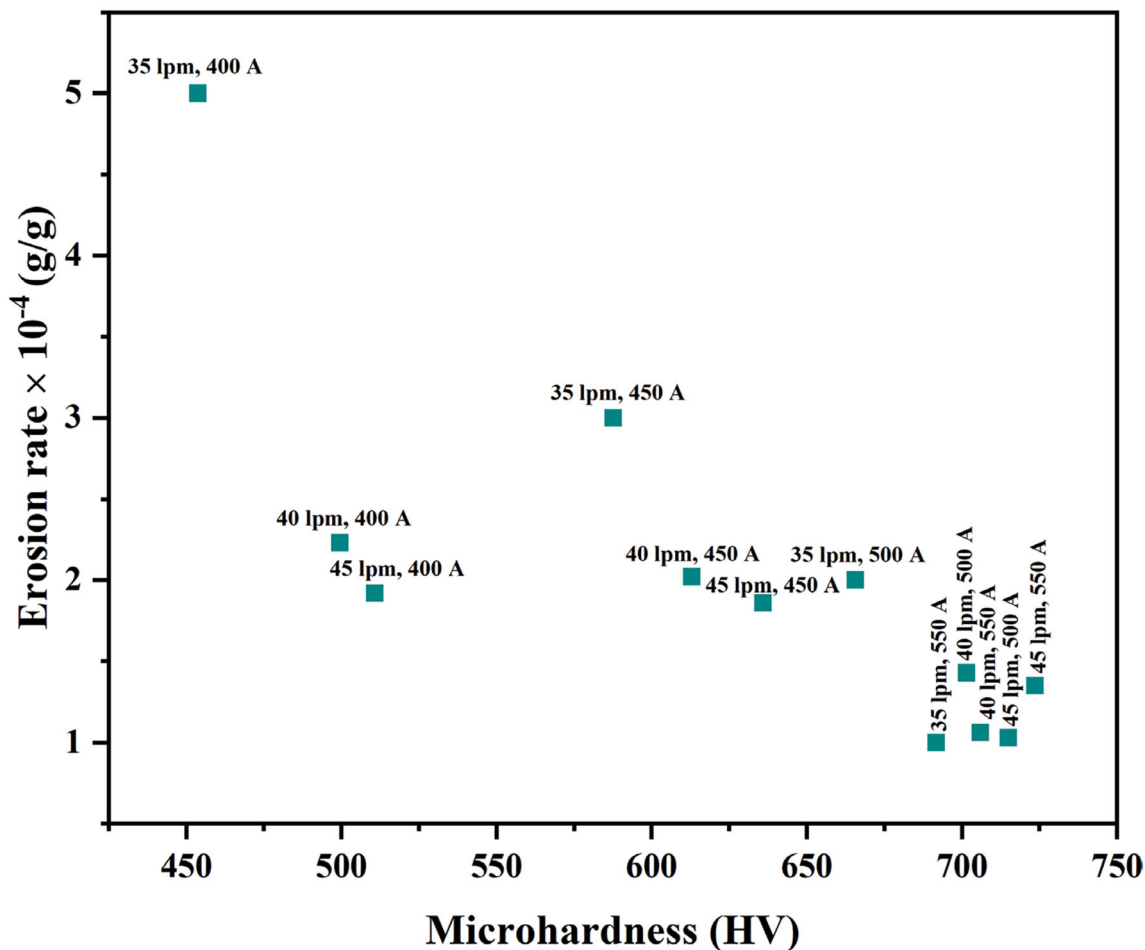


Fig. 18 Relation between microhardness and erosion rate of the plasma sprayed NiTi coating with impinged erodent angle of 45°

high impact energy of the vertical component of the erodent particle. In addition to the above, the impact of the erodent particles on the splat boundaries resulted in splat fragmentation or splat delamination. The strike of erodent normally on the microcracks also leads to the splat fracture on the coating surface. The pit formation occurs due to the repeated impingement of the erodent on the coating surface.

Conclusions

In the current investigation, the NiTi coatings have been developed on the mild steel substrate using atmospheric plasma spray technique. The solid particle erosion

performance of the coatings has been investigated and the effect of coating properties on the erosion performance of the coating have been analyzed. Based on the obtained results, the following conclusions have been made:

- The developed coatings consist of various phases such as NiTi-B2 phase, Ni_3Ti , Ti_2Ni , Ni, Ti, NiO, TiO and Ni_4Ti_3 . These phases have been confirmed by EDS analysis. The SEM morphologies of the coating surfaces and interfaces depicted the presence of surface (surface microcracks, unmelted/partially melted particles, surface pores, splat fracture, etc.) and interfacial defects (porosity, inter-lamellar cracks, vertical cracks, inter-splat cracks, etc.) at lower primary gas flow rate and plasma arc current.

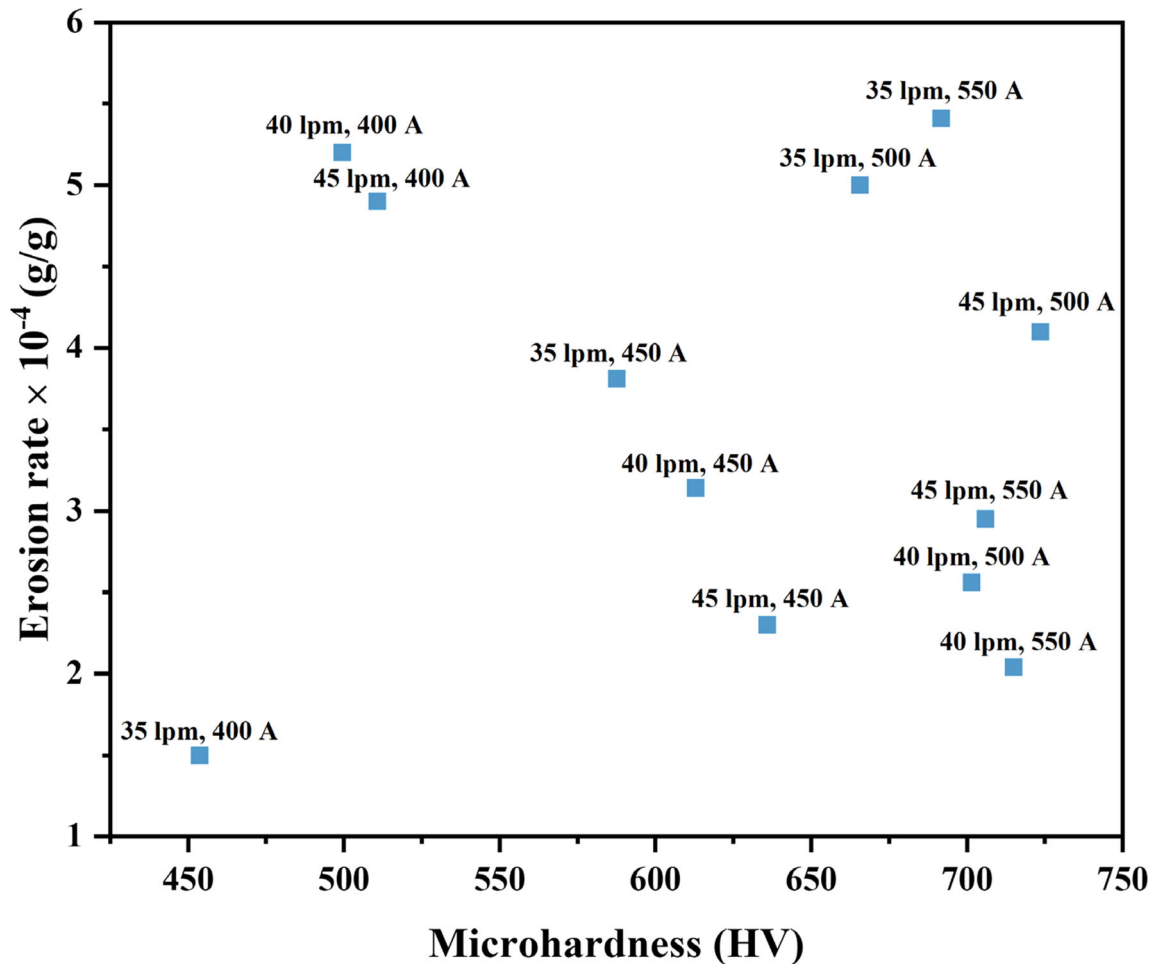


Fig. 19 Relation between microhardness and erosion rate of the plasma sprayed NiTi coating with impinged erodent angle of 90°

- The porosity investigation revealed that at lower primary gas flow rate and lower arc current, the porosity percentage is more due to the more unmelted particles, air and inclusions entrapment within the deposited layers. The unmelted particles formation, inhomogeneous deposition and low plasma column resulted in the higher surface roughness of the coatings. Furthermore, the microhardness of the coatings is reduced at lower plasma arc current and primary gas flow rate due to the thermal pinching effect and low enthalpy generation.
- The presence of surface defects leads to the easier penetration of the erodent in the coating and, hence, facilitate in the material removal process. Furthermore, the austenitic phase NiTi-B2 has a higher erosion resistance due to the superelasticity property and the accumulation of little strain. Again, Ti₂Ni phase contributes to the enhancement of hardness and, hence, contributes to erosion performance.
- The erosion rate of the coatings increases with increase in porosity percentage in both the erodent impingement angles (45° and 90°). This is due to the lack of strength at the edges of the pores/voids and weak inter-lamellar strength developed due to the presence of porosity. The porosity also acts like a stress concentrator which leads to the easy failure of the coating at erosion environment.
- In most of the cases, the erosion rate of the plasma sprayed coatings is higher at higher surface roughness. The surface area of the roughness peaks, the stress

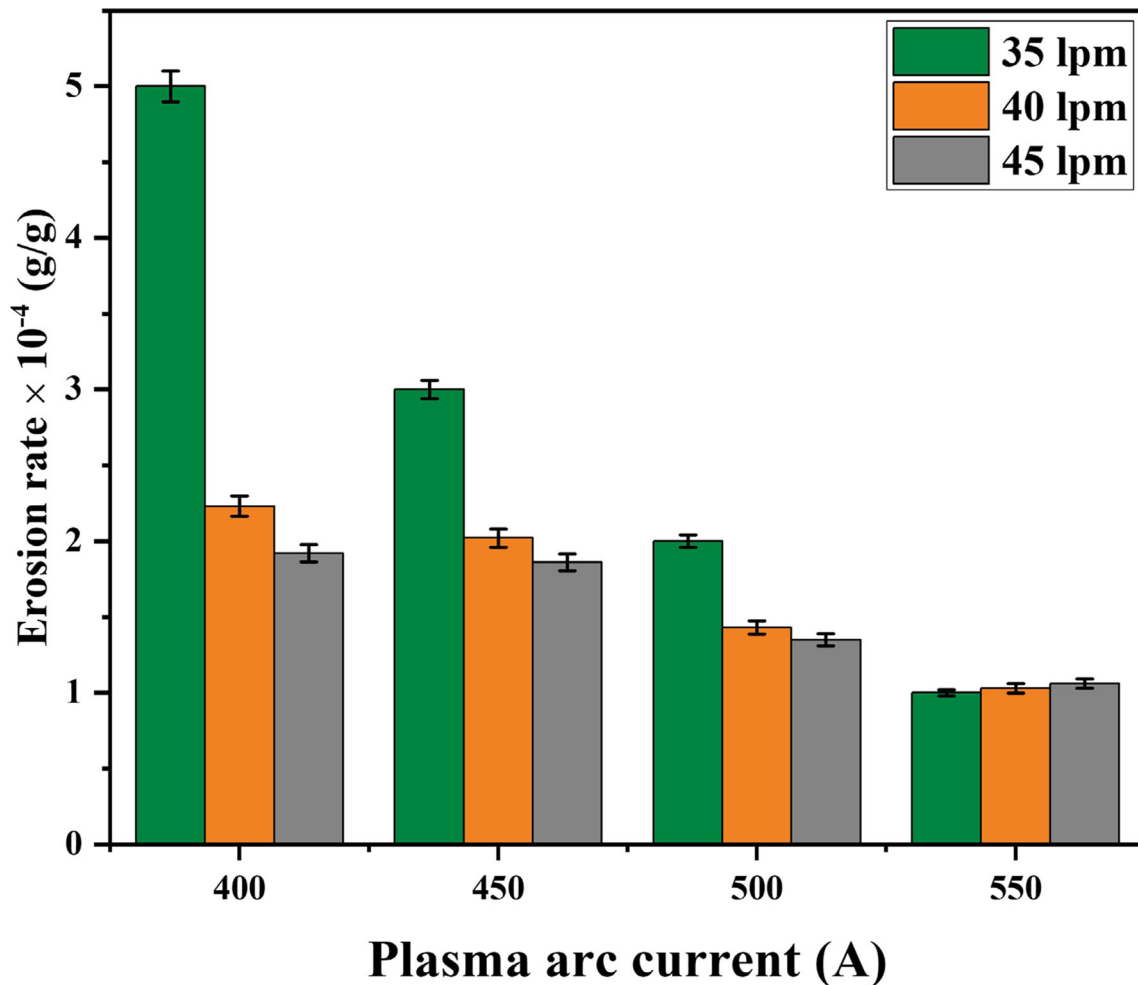


Fig. 20 The erosion of the coatings impinged at 45° impingement angle

concentration at the gap between the roughness peaks and height of the surface profile play a vital role in the erosion phenomenon.

- The erosion rate decreases with increase in microhardness value of the coating due to inability of some of the erodent particles to penetrate the coating surface and rebound from the surface. Again, in some of the cases, the erosion rate increases with increase in microhardness value which is expected to be due to the effect of pseudoelasticity property of the coating.
- The more erosion rate has been observed in the coatings impinged at 90° impingement angle, and it has been concluded that the coating is little brittle in nature. The SEM morphologies of the coatings impinged at 45° and 90° impingement angles indicate various wear mechanisms like plastic deformation, plowing, microcutting, lip formation, scratches, groove formation in 45° impingement angle and groove formation, splat fracture, splat fragmentation, splat delamination, pit formation in 90° impingement angle of the erodent.

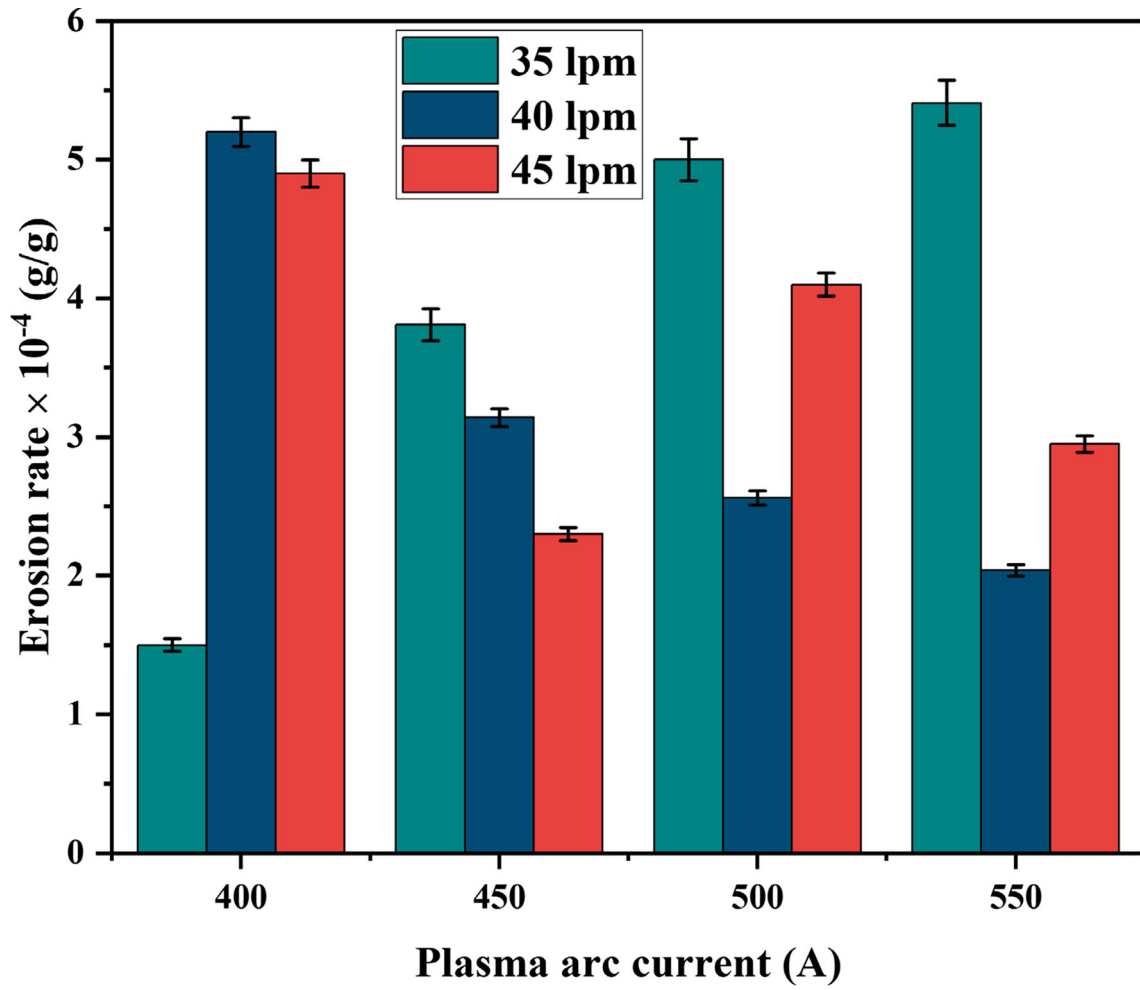


Fig. 21 The erosion of the coatings impinged at 90° impingement angle

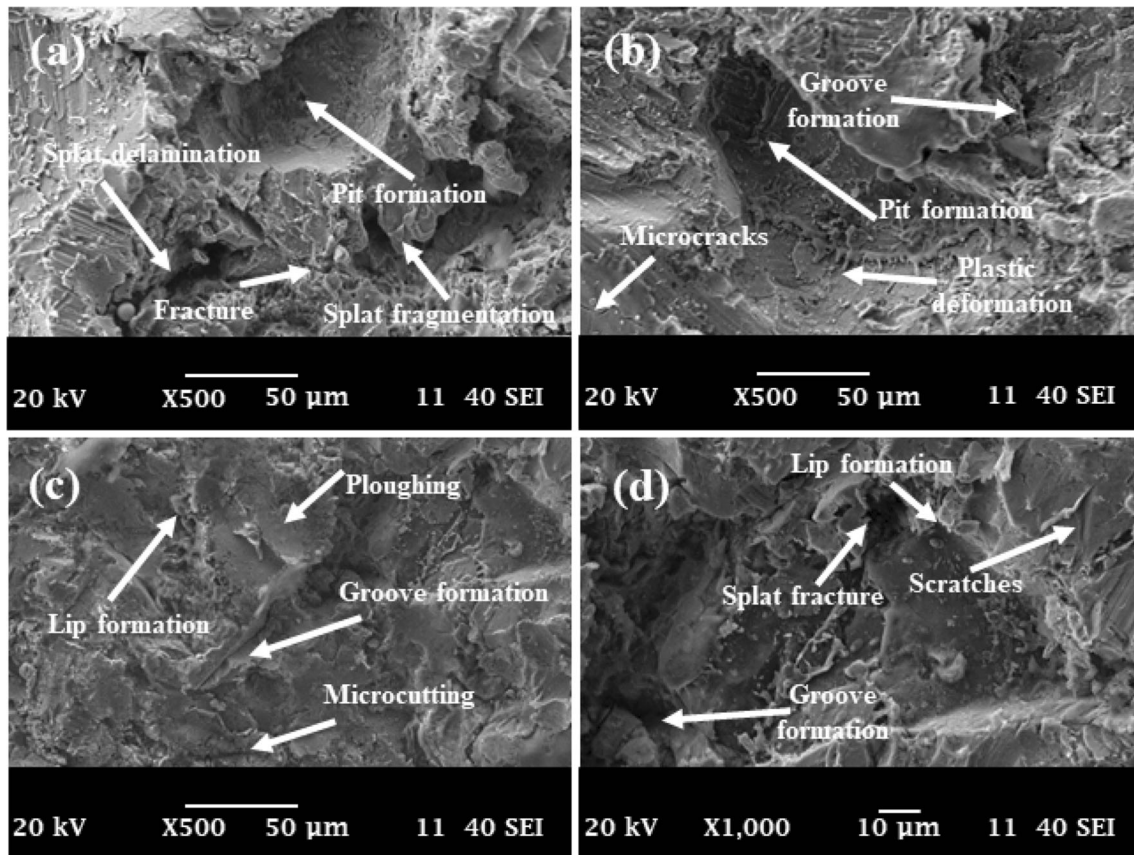


Fig. 22 Surface morphologies of eroded coating samples at 90° (a and b) and 45° (c and d)

References

- M. Pepi, R. Squillacioti, L. Pfluederer and A. Phelps, Solid Particle Erosion Testing of Helicopter Rotor Blade Materials, *J. Fail. Anal. Prev.*, 2012, **12**(1), p 96-108. <https://doi.org/10.1007/s11668-011-9531-3>
- J. Alqallaf, N. Ali, J.A. Teixeira and A. Addali, Solid Particle Erosion Behaviour and Protective Coatings for Gas Turbine Compressor Blades-A Review, *Processes*, 2020, **8**(8), p 984. <https://doi.org/10.3390/pr8080984>
- B. Swain, P. Mallick, S. Patel, R. Roshan, S.S. Mohapatra, S. Bhuyan, M. Priyadarshini, B. Behera, S. Samal and A. Behera, Failure Analysis and Materials Development of Gas Turbine Blades, *Mater. Today Proc.*, 2020 <https://doi.org/10.1016/j.matpr.2020.02.859>
- J.R. Laguna-camacho, L.Y. Villagrán-villegas, H. Martínez-garcía and G. Juárez-morales, A Study of the Wear Damage on Gas Turbine Blades, *EFA*, 2016, **61**, p 88-99. <https://doi.org/10.1016/j.engfailanal.2015.10.002>
- A.A. Hamed, W. Tabakoff, R.B. Rivir, K. Das and P. Arora, Turbine Blade Surface Deterioration by Erosion, *J. Turbomach.*, 2005, **127**(3), p 445. <https://doi.org/10.1115/1.1860376>
- S. Benterki, A. Faci and N. Bouaouadja, A Windshields Surface Characterization Damaged by Sandblasting, *Int. J. Appl. Glas. Sci.*, 2020, **11**(2), p 245-252. <https://doi.org/10.1111/ijag.14584>
- R.C. Sirs, "The Operation of Gas Turbine Engines in Hot & Sandy Conditions-Royal Air Force Experiences in the Gulf War," in: *AGARD Conference Proceedings*, 1994, p 2-1
- M. Selinger, "Pratt & Whitney Modifying Lead Engine for JSF,"(2007) <http://www.aviationweek.com>
- S. Kumar Patel, B. Swain, R. Roshan, N.K. Sahu and A. Behera, A Brief Review of Shape Memory Effects and Fabrication Processes of NiTi Shape Memory Alloys, *Mater. Today Proc.*, 2020, **33**, p 5552-5556. <https://doi.org/10.1016/j.matpr.2020.03.539>
- S.K. Patel, B. Behera, B. Swain, R. Roshan, D. Sahoo and A. Behera, A Review on NiTi Alloys for Biomedical Applications and Their Biocompatibility, *Mater. Today Proc.*, 2020, **33**, p 5548-5551. <https://doi.org/10.1016/j.matpr.2020.03.538>
- Y. Oshida and S. Miyazaki, Corrosion and Biocompatibility of Shape Memory Alloys, *Zairyo-to-Kankyo*, 1991, **40**(12), p 834-844. <https://doi.org/10.3323/jcorr1991.40.834>
- P. Clayton, Tribological Behavior of a Titanium-Nickel Alloy, *Wear*, 1993, **162-164**, p 202-210. [https://doi.org/10.1016/0043-1648\(93\)90502-D](https://doi.org/10.1016/0043-1648(93)90502-D)
- H.C. Lin, H.M. Liao, J.L. He, K.C. Chen and K.M. Lin, Wear Characteristics of TiNi Shape Memory Alloys, *Metall. Mater. Trans. A*, 2000, **28**(9), p 1871-1877.
- Y. Shida and Y. Sugimoto, Water Jet Erosion Behaviour of Ti-Ni Binary Alloys, *Wear*, 1991, **146**(2), p 219-228.
- A.P. Jardine, Y. Field and H. Herman, Shape Memory Effect in Vacuum Plasma Sprayed NiTi, *J. Mater. Sci. Lett.*, 1991, **10**(16), p 943-945. <https://doi.org/10.1007/BF00722140>
- H.C. Lin, S.K. Wu and M.T. Yeh, Damping Characteristics of TiNi Shape Memory Alloys, *Metall. Trans. A*, 1993, **24**(10), p 2189-2194. <https://doi.org/10.1007/BF02648593>
- K. Melton and O. Mercier, Fatigue of NITI Thermoelastic Martensites, *Acta Metall.*, 1979, **27**(1), p 137-144. [https://doi.org/10.1016/0001-6160\(79\)90065-8](https://doi.org/10.1016/0001-6160(79)90065-8)
- R. Westergård, L.C. Erickson, N. Axén, H.M. Hawthorne and S. Hogmark, The Erosion and Abrasion Characteristics of Alumina Coatings Plasma Sprayed under Different Spraying Conditions, *Tribol. Int.*, 1998, **31**(5), p 271-279.
- D. Toma, W. Brandl and G. Marginean, Wear and Corrosion Behaviour of Thermally Sprayed Cermet Coatings, *Surf. Coat. Technol.*, 2001, **138**(2-3), p 149-158.
- Y. Fu, A.W. Batchelor, Y. Wang and K.A. Khor, Fretting Wear Behaviors of Thermal Sprayed Hydroxyapatite (HA) Coating under Unlubricated Conditions, *Wear*, 1998, **217**(1), p 132-139.
- H. Liao, B. Normand and C. Coddet, Influence of Coating Microstructure on the Abrasive Wear Resistance of WC/Co Cermet Coatings, *Surf. Coat. Technol.*, 2000, **124**(2-3), p 235-242.
- B. Swain and A. Behera, Effect of Powder Feed Rate on Adhesion Strength and Microhardness of APS NiTi Coating: A Microstructural Investigation, *Surf. Topogr. Metrol. Prop.*, 2021, **9**(2), p 025039. <https://doi.org/10.1088/2051-672X/ac0a38>
- P. Mallick, B. Behera, S.K. Patel, B. Swain, R. Roshan and A. Behera, Plasma Spray Parameters to Optimize the Properties of Abrasion Coating Used in Axial Flow Compressors of Aero-Engines to Maintain Blade Tip Clearance, *Mater. Today Proc.*, 2020, **33**, p 5691-5697. <https://doi.org/10.1016/j.matpr.2020.03.835>
- S. Sampath, U. Schulz, M.O. Jarligo and S. Kuroda, Processing Science of Advanced Thermal-Barrier Systems, *MRS Bull.*, 2012, **37**(10), p 903-910.
- B. Swain, S. Bhuyan, R. Behera, S.S. Mohapatra and A. Behera, Wear: A Serious Problem in Industry, *Tribology in Materials and Manufacturing-Wear, Friction and Lubrication*. A. Patnaik, T. Singh, V. Kukshal Ed., IntechOpen, London, 2021. <https://doi.org/10.5772/intechopen.94211>
- H. Herman, Plasma-Sprayed Coatings, *Sci. Am.*, 1988, **259**(3), p 112-117.
- S. Lathabai, M. Ottmüller and I. Fernandez, Solid Particle Erosion Behaviour of Thermal Sprayed Ceramic, *Met. Polym. Coat. Wear*, 1998, **221**(2), p 93-108.
- B. Swain, S. Chatterjee, S.S. Mohapatra, and A. Behera, Mechanical Properties Evaluation and Parametric Optimization of Atmospheric Plasma Spray NiTi Coating, *J. Mater. Eng. Perform.*, 2022, p 1-15 <https://doi.org/10.1007/s11665-022-06834-0>
- B. Swain, S. Kumar Bhuyan, S. Sanjeeb Mohapatra, D. Kumar Rajak, A. Behera and C. Iulian Pruncu, Adhesion Strength Investigation of Plasma Sprayed NiTi Coating, *Eng. Fail. Anal.*, 2022, **140**, p 106368. <https://doi.org/10.1016/j.engfailanal.2022.106368>
- B. Swain, A.R. Pati, S.S. Mohapatra and A. Behera, Interchanging Characteristic of Plasma Spray Coating from Superhydrophobic to Hydrophilic under the Applied Electric Field, *Surface Engineering*, 2021, **37**(10), p 1328-1337. <https://doi.org/10.1080/02670844.2021.1959286>
- B. Swain, P. Mallick, S.S. Mohapatra, A. Behera, D.K. Rajak and P.L. Menezes, Atmospheric Plasma Spray Coating of NiTi on Mild Steel Substrate: An Microstructural Investigation, *J. Bio-Tribo-Corros.*, 2021, **7**(3), p 104. <https://doi.org/10.1007/s40735-021-00541-4>
- B. Swain, A.R. Pati, P. Mallick, S.S. Mohapatra and A. Behera, Development of Highly Durable Superhydrophobic Coatings by One-Step Plasma Spray Methodology, *J. Therm. Spray Technol.*, 2021, **30**(1-2), p 405-423. <https://doi.org/10.1007/s11666-020-01132-4>
- B. Swain, S. Patel, P. Mallick, S.S. Mohapatra, and A. Behera, "Solid Particle Erosion Wear of Plasma Sprayed NiTi Alloy Used for Aerospace Applications,". in: *Proceedings of the International Thermal Spray Conference*, 2019, p 346-351
- N. Cinca, A. Isalgue, J. Fernández and J.M. Guilemany, Structure Characterization and Wear Performance of NiTi Thermal Sprayed Coatings, *Smart Mater. Struct.*, 2010, **19**(8), p 085011. <https://doi.org/10.1088/0964-1726/19/8/085011>
- H. Hiraga, T. Inoue, H. Shimura and A. Matsunawa, Cavitation Erosion Mechanism of NiTi Coatings Made by Laser Plasma

- Hybrid Spraying, *Wear*, 1999, **231**(2), p 272–278. [https://doi.org/10.1016/S0043-1648\(99\)00133-7](https://doi.org/10.1016/S0043-1648(99)00133-7)
36. J.M. Guilemany, N. Cinca, S. Dosta and A.V. Benedetti, Corrosion Behaviour of Thermal Sprayed Nitinol Coatings, *Corros. Sci.*, 2009, **51**(1), p 171–180. <https://doi.org/10.1016/j.corsci.2008.10.022>
 37. Z. Shi, J. Wang, Z. Wang, Y. Qiao, T. Xiong and Y. Zheng, Cavitation Erosion and Jet Impingement Erosion Behavior of the NiTi Coating Produced by Air Plasma Spraying, *Coatings*, 2018, **8**(10), p 346. <https://doi.org/10.3390/coatings8100346>
 38. B. Swain, P. Mallick, S.K. Bhuyan, S.S. Mohapatra, S.C. Mishra and A. Behera, Mechanical Properties of NiTi Plasma Spray Coating, *J. Therm. Spray Technol.*, 2020, **29**(4), p 741–755. <https://doi.org/10.1007/s11666-020-01017-6>
 39. B. Swain, S. Bajpai and A. Behera, Microstructural Evolution of NITINOL and Their Species Formed by Atmospheric Plasma Spraying, *Surf. Topogr. Metrol. Prop.*, 2019, **7**(1), p 601500. <https://doi.org/10.1088/2051-672X/aaf30e>
 40. B. Swain, P. Mallick, R.K. Gupta, S.S. Mohapatra, G. Yasin, T.A. Nguyen and A. Behera, Mechanical and Tribological Properties Evaluation of Plasma-Sprayed Shape Memory Alloy Coating, *J. Alloys Compd.*, 2021, **863**, p 158599. <https://doi.org/10.1016/j.jallcom.2021.158599>
 41. B. Swain, M. Priyadarshini, S.S. Mohapatra, R.K. Gupta and A. Behera, Parametric Optimization of Atmospheric Plasma Spray Coating Using Fuzzy TOPSIS Hybrid Technique, *J. Alloys Compd.*, 2021, **867**, p 159074. <https://doi.org/10.1016/j.jallcom.2021.159074>
 42. M.M. Verdian, K. Raeissi and M. Salehi, Corrosion Performance of HVOF and APS Thermally Sprayed NiTi Intermetallic Coatings in 3.5% NaCl Solution, *Corros. Sci.*, 2010, **52**(3), p 1052–1059. <https://doi.org/10.1016/j.corsci.2009.11.034>
 43. S. Sampath and H. Herman, Rapid Solidification and Microstructure Development during Plasma Spray Deposition, *J. Therm. Spray Technol.*, 1996, **5**(4), p 445–456.
 44. M.M. Verdian, K. Raeissi and M. Salehi, Electrochemical Impedance Spectroscopy of HVOF-Sprayed NiTi Intermetallic Coatings Deposited on AISI 1045 Steel, *J. Alloys Compd.*, 2010, **507**(1), p 42–46. <https://doi.org/10.1016/j.jallcom.2010.07.132>
 45. D.G. Bhosale, T.R. Prabhu, W.S. Rathod, M.A. Patil and S.W. Rukhande, High Temperature Solid Particle Erosion Behaviour of SS 316L and Thermal Sprayed WC-Cr3C2-Ni Coatings, *Wear*, 2020, **462–463**, p 203520. <https://doi.org/10.1016/j.wear.2020.203520>
 46. V. Singh, I. Singh, A. Bansal, A. Omer, A.K. Singla and D.K. Goyal, Cavitation Erosion Behavior of High Velocity Oxy Fuel (HVOF) Sprayed (VC+ CuNi-Cr) Based Novel Coatings on SS316 Steel, *Surf. Coat. Technol.*, 2022, **432**, p 128052. <https://doi.org/10.1016/j.surfcoat.2021.128052>
 47. K. Otsuka and X. Ren, Physical Metallurgy of Ti-Ni-Based Shape Memory Alloys, *Prog. Mater. Sci.*, 2005, **50**(5), p 511–678.
 48. “Nickel Titanium-Wikipedia,” n.d., https://en.wikipedia.org/wiki/Nickel_titanium. (Accessed 2 December 2019)
 49. M. Bram, A. Ahmad-Khanlou, H.P. Buchkremer and D. Stöver, Vacuum Plasma Spraying of NiTi Protection Layers, *Mater. Lett.*, 2002, **57**(3), p 647–651.
 50. L. Gao, H. Guo, L. Wei, C. Li, S. Gong and H. Xu, Microstructure and Mechanical Properties of Yttria Stabilized Zirconia Coatings Prepared by Plasma Spray Physical Vapor Deposition, *Ceram. Int.*, 2015, **41**(7), p 8305–8311. <https://doi.org/10.1016/j.ceramint.2015.02.141>
 51. O. Sarikaya, E. Celik, S.C. Okumus, S. Aslanlar and S. Anik, Effect on Residual Stresses in Plasma Sprayed Al-Si/B4C Composite Coatings Subjected to Thermal Shock, *Surf. Coat. Technol.*, 2005, **200**(7), p 2497–2503. <https://doi.org/10.1016/j.surfcoat.2004.08.071>
 52. D. Thirumalaikumarasamy, K. Shanmugam and V. Balasubramanian, Establishing Empirical Relationships to Predict Porosity Level and Corrosion Rate of Atmospheric Plasma-Sprayed Alumina Coatings on AZ31B Magnesium Alloy, *J. Magnes. Alloy.*, 2014, **2**(2), p 140–153. <https://doi.org/10.1016/j.jma.2014.05.002>
 53. P. Ctibor, R. Lechnerová and V. Beneš, Quantitative Analysis of Pores of Two Types in a Plasma-Sprayed Coating, *Mater. Charact.*, 2006, **56**(4–5), p 297–304. <https://doi.org/10.1016/j.matchar.2005.11.016>
 54. I.Y. Konyashin and T.V. Chukalovskaya, A Technique for Measurement of Porosity in Protective Coatings, *Surf. Coat. Technol.*, 1997, **88**(1–3), p 5–11. [https://doi.org/10.1016/S0257-8972\(95\)02758-0](https://doi.org/10.1016/S0257-8972(95)02758-0)
 55. R. Jůzková, P. Ctibor and V. Beneš, Analysis of Porous Structure in Plasma-Sprayed Coating, *Image Anal. Stereol.*, 2011, **23**(1), p 45. <https://doi.org/10.5566/ias.v23.p45-52>
 56. J. Huang, W. Wang, X. Lu, S. Liu and C. Li, Influence of Lamellar Interface Morphology on Cracking Resistance of Plasma-Sprayed YSZ Coatings, *Coatings*, 2018, **8**(5), p 187. <https://doi.org/10.3390/coatings8050187>
 57. E.A. Zverev, V.Y. Skeebe, P.Y. Skeebe and I.V. Khlebova, Defining Efficient Modes Range for Plasma Spraying Coatings, *IOP Conf. Ser. Earth Environ. Sci.*, 2017, **87**(8), p 082061. <https://doi.org/10.1088/1755-1315/87/8/082061>
 58. J.G. Odhiambo, W. Li, Y. Zhao and C. Li, Porosity and Its Significance in Plasma-Sprayed Coatings, *Coatings*, 2019, **9**(7), p 460. <https://doi.org/10.3390/coatings9070460>
 59. G. Mauer, Plasma Characteristics and Plasma-Feedstock Interaction under PS-PVD Process Conditions, *Plasma Chem. Plasma Process.*, 2014, **34**(5), p 1171–1186. <https://doi.org/10.1007/s11090-014-9563-z>
 60. X. Zhang, C. Wang, R. Ye, C. Deng, X. Liang, Z. Deng, S. Niu, J. Song, G. Liu, M. Liu, K. Zhou, J. Lu and J. Feng, Mechanism of Vertical Crack Formation in Yb2SiO5 Coatings Deposited via Plasma Spray-Physical Vapor Deposition, *J. Mater.*, 2020, **6**(1), p 102–108. <https://doi.org/10.1016/j.jmat.2020.01.002>
 61. R. Ghasemi and H. Vakili-fard, Plasma-Sprayed Nanostructured YSZ Thermal Barrier Coatings: Thermal Insulation Capability and Adhesion Strength, *Ceram. Int.*, 2017, **43**(12), p 8556–8563. <https://doi.org/10.1016/j.ceramint.2017.03.074>
 62. M. Hajian Foroushani, M. Shamanian, M. Salehi and F. Davar, Porosity Analysis and Oxidation Behavior of Plasma Sprayed YSZ and YSZ/LaPO4 Abradable Thermal Barrier Coatings, *Ceram. Int.*, 2016, **42**(14), p 15868–15875. <https://doi.org/10.1016/j.ceramint.2016.07.057>
 63. J.A. Curran and T.W. Clyne, Porosity in Plasma Electrolytic Oxide Coatings, *Acta Mater.*, 2006, **54**(7), p 1985–1993. <https://doi.org/10.1016/j.actamat.2005.12.029>
 64. A.H. Pakseresht, E. Ghasali, M. Nejati, K. Shirvanimoghaddam, A.H. Javadi and R. Teimouri, Development Empirical-Intelligent Relationship between Plasma Spray Parameters and Coating Performance of Yttria-Stabilized Zirconia, *Int. J. Adv. Manuf. Technol.*, 2014, **76**(5–8), p 1031–1045.
 65. R.H. Richman, A.S. Rao and D.E. Hodgson, Cavitation Erosion of Two NiTi Alloys, *Wear*, 1992, **157**(2), p 401–407.
 66. Y. Maozhong, H. Baiyun and H. Jiawen, Erosion Wear Behaviour and Model of Abradable Seal Coating, *Wear*, 2002, **252**(1–2), p 9–15. [https://doi.org/10.1016/S0043-1648\(01\)00681-0](https://doi.org/10.1016/S0043-1648(01)00681-0)
 67. J. Hearley, J. Little and A. Sturgeon, The Erosion Behaviour of NiAl Intermetallic Coatings Produced by High Velocity Oxy-Fuel Thermal Spraying, *Wear*, 1999, **233–235**, p 328–333. [https://doi.org/10.1016/S0043-1648\(99\)00240-9](https://doi.org/10.1016/S0043-1648(99)00240-9)
 68. P.K. Singh and S.B. Mishra, Erosion Wear Characteristics of HVOF Sprayed WC-Co-Cr and CoNiCrAlY Coatings on IS-2062 Structural Steel, *Mater. Res. Express*, 2018, **5**(9), p 095508. <https://doi.org/10.1088/2053-1591/aad85d>

69. A. Patnaik, A. Satapathy, N. Chand, N.M. Barkoula and S. Biswas, Solid Particle Erosion Wear Characteristics of Fiber and Particulate Filled Polymer Composites: A Review, *Wear*, 2010, **268**(1-2), p 249-263. <https://doi.org/10.1016/j.wear.2009.07.021>
70. N. Krishnamurthy, M.S. Murali, B. Venkataraman and P.G. Mukunda, Characterization and Solid Particle Erosion Behavior of Plasma Sprayed Alumina and Calcia-Stabilized Zirconia Coatings on Al-6061 Substrate, *Wear*, 2012, **274-275**, p 15-27.
71. P. Kulu, I. Hussainova and R. Veinthal, Solid Particle Erosion of Thermal Sprayed Coatings, *Wear*, 2005, **258**(1-4), p 488-496.
72. Y. Maozhong, H. Baiyun and H. Jiawen, Erosion Wear Behaviour and Model for Abradable Seal Coating, *Wear*, 2002, **252**(1-2), p 9-15.
73. B. Wang, Erosion-Corrosion of Thermal Sprayed Coatings in FBC Boilers, *Wear*, 1996, **199**(1), p 24-32. [https://doi.org/10.1016/0043-1648\(96\)06972-4](https://doi.org/10.1016/0043-1648(96)06972-4)
74. B. Wang and S.W. Lee, Erosion-Corrosion Behaviour of HVOF NiAl-Al₂O₃ Intermetallic-Ceramic Coating, *Wear*, 2000, **239**(1), p 83-90. [https://doi.org/10.1016/S0043-1648\(00\)00309-4](https://doi.org/10.1016/S0043-1648(00)00309-4)
75. B.Q. Wang and Z.R. Shui, The Hot Erosion Behavior of HVOF Chromium Carbide-Metal Cermet Coatings Sprayed with Different Powders, *Wear*, 2002, **253**(5-6), p 550-557. [https://doi.org/10.1016/S0043-1648\(02\)00049-2](https://doi.org/10.1016/S0043-1648(02)00049-2)
76. H. Singh and B.S. Sidhu, Erosion Characteristics of HVOF Developed Cr₃C₂-NiCr and WC-Co Coatings, *Mater. Sci. Forum*, 2013, **751**, p 71-79. <https://doi.org/10.4028/www.scientific.net/MSF.751.71>
77. H.S. Sidhu, B.S. Sidhu and S. Prakash, Solid Particle Erosion of HVOF Sprayed NiCr and Stellite-6 Coatings, *Surf. Coat. Technol.*, 2007, **202**(2), p 232-238. <https://doi.org/10.1016/j.surfcoat.2007.05.035>

Publisher's Note Springer Nature remains neutral with regard to jurisdictional claims in published maps and institutional affiliations.

Springer Nature or its licensor holds exclusive rights to this article under a publishing agreement with the author(s) or other rightsholder(s); author self-archiving of the accepted manuscript version of this article is solely governed by the terms of such publishing agreement and applicable law.